Cell Biol Toxicol (2025) 41:86
https://doi.org/10.1007/s10565-025-10035-5

RESEARCH

Neuron-like macrophage differentiation via the APOE-TREM2 axis contributes to chronic pain in nasopharyngeal carcinoma

Hongxi Li · Lanqing Zhao · Jinwei Li · Kailin Zhang · Weiliang Bai · Yu Chen

Received: 1 November 2024 / Accepted: 24 April 2025

Abstract Chronic pain is a prevalent and debilitating symptom in patients with nasopharyngeal carcinoma (NPC). Fresh insights indicate that tumor-associated macrophages (TAMs) within the tumor microenvironment (TME) may undergo neuron-like differentiation, potentially contributing to pain mechanisms. By examining the *apolipoprotein E (APOE)* together with the *triggering receptor expressed on myeloid cells 2 (TREM2)*, this study aims to clarify their joint function in modulating differentiation and how this interplay might be implicated in chronic pain associated with NPC. Through comprehensive analysis using TCGA-NPC transcriptomic datasets and single-cell RNA sequencing (scRNA-seq), we assessed the molecular landscapes of both NPC-affected and healthy nasopharyngeal tissues. Differential gene expression and immune cell profiling identified macrophages as key players in the inflammatory response. Single-cell sequencing revealed a distinct subpopulation of neuron-like macrophages expressing neurogenesis-related genes. Macrophage-to-neuron-like cell transformation in response to NPC cells was examined through *in vitro* co-culture systems, highlighting the involvement of the APOE-TREM2 regulatory pathway. *In vivo* studies involved macrophage depletion and TREM2 knockdown in mouse models to evaluate the impact on chronic pain development. Infiltrating macrophages were significantly more abundant in NPC samples, with many exhibiting neuron-like features that were positively linked to high levels of *WNT5 A* expression. *In vitro*, NPC cells induced macrophage differentiation into

Hongxi Li, Lanqing Zhao, Jinwei Li and Kailin Zhang are regarded as co-first authors.

Supplementary Information The online version contains supplementary material available at https://doi.org/10.1007/s10565-025-10035-5.

H. Li
Department of Pain Management, Shengjing Hospital of China Medical University, Shenyang 110000, China

L. Zhao
Department of Sleep Medicine Center, Shengjing Hospital of China Medical University, Shenyang 110000, Liaoning, PR China

J. Li
Department of Neurology/Stroke Center, the First Affiliated Hospital of China Medical University, Shenyang 110000, Liaoning, PR China

K. Zhang
Department of Ion Channel Pharmacology, School of Pharmacy, China Medical University, Shenyang 110122, China

W. Bai (✉) · Y. Chen (✉)
Department of Otolaryngology Head and Neck Surgery, Shengjing Hospital of China Medical University, No.39, Huaxiang Road, Tiexi District, Shenyang 110000, Liaoning, China
e-mail: bweiliangcmu@163.com

Y. Chen
e-mail: lihx@sj-hospital.org

Published online: 20 May 2025

neuron-like cells, a process regulated by *TREM2* and *APOE*. TREM2 knockdown in macrophages resulted in a reduction of chronic pain behaviors in mouse models, highlighting the contribution of the APOE-TREM2 Axis to NPC-associated chronic pain. Our findings demonstrate that NPC cells promote macrophage reprogramming through the APOE-TREM2 Axis, leading to neuron-like differentiation and contributing to chronic pain in NPC patients. Targeting this pathway may offer novel therapeutic strategies for managing chronic pain in NPC.

Keywords Nasopharyngeal carcinoma · Chronic pain · Single-cell sequencing · TCGA · Neuron-like macrophages · TREM2

Introduction

Nasopharyngeal carcinoma (NPC) is a prevalent malignant tumor located in the head and neck region, primarily prevalent in Asia and North Africa (Zhang et al. 2022; Chang et al. 2021). Despite advancements in the diagnosis and treatment techniques for NPC in recent years, numerous patients continue to experience various complications during and after treatment. Chronic pain, often overlooked, represents an issue (Li et al. 2022). The presence of sustained pain can significantly impair life satisfaction and may correlate with heightened risks of tumor resurgence and dissemination (Wang et al. 2025; Yassen et al. 2024). Despite limited insights into the molecular basis of pain, accumulating evidence points to the tumor microenvironment (TME) as a potentially significant contributor to its onset (Cohen et al. 2021).

The biological architecture of the TME integrates a range of cell types, such as neoplastic cells, immune cells, connective tissue fibroblasts, and vascular endothelial cells, forming a highly complex system (Yan et al. 2021; Xiao and Yu 2021). These cells communicate with one another by secreting cytokines, chemical factors, and other substances, collectively impacting the growth, progression, and metastasis of tumors (Viswanadhapalli et al. 2022). Recent studies have provided increasing evidence indicating that specific immune cells, particularly macrophages, may significantly contribute to the pathogenesis of chronic pain in individuals diagnosed with NPC (Wang et al. 2023a; Liu et al. 2021). However, the exact workings of the mechanism remain unclear. Studies have shown that in post-mastectomy pain syndrome, chronic neuropathic pain following nerve injury is closely related to nerve fiber damage, and macrophages serve essential functions in both the immune-mediated inflammatory cascade and in mechanisms of neural repair (Zhang et al. 2023). Furthermore, in neuropathic pain models, such as paclitaxel-induced neuropathic pain, the interaction between macrophage activation and neuronal damage has been extensively studied, revealing the potential role of macrophages in pain signal transmission (Klein and Lehmann 2021). These findings suggest that macrophage-neuron interactions are prevalent in various chronic pain conditions and may influence pain perception through different mechanisms.

Single-cell sequencing technology provides a powerful tool for exploring different cell types and subpopulations within the TME. It enables us to analyze the transcriptome of individual cells (Caushi et al. 2021). Furthermore, publicly available databases, such as TCGA-NPC, provide a vast amount of genomic, transcriptomic, and proteomic data that serve as valuable resources for investigating the correlation between macrophages and chronic pain in NPC (Zhu et al. 2024; Chen et al. 2024). By integrating these two techniques, we could enhance our comprehension of macrophage heterogeneity in the TME and its influence on chronic pain in those suffering from NPC.

The purpose of this research is to dissect the potential biological processes, using single-cell and transcriptome sequencing, through which a distinct group of neuron-like macrophages in the TME might influence chronic pain progression in NPC. This investigation focuses on delivering new insights into therapeutic solutions and intervention targets for more effective chronic pain management in the context of NPC. Furthermore, these findings offer valuable insights into comprehending the correlation between other types of malignant tumors and chronic pain, thereby positing critical scientific and clinical implications.

Materials and methods

Ethics statement

Ethical permission to carry out the current research was issued by the Shengjing Hospital Ethics

Committee, China Medical University. Before the commencement of the Experiment, all participants were thoroughly briefed on the objectives and potential hazards involved. Subsequently, they provided written informed consent. Furthermore, we guarantee the privacy and confidentiality of the personal information of participants. In regards to animal experiments, all experiments strictly adhere to the"Guidelines for Animal Experiment Ethics". It includes but is not limited to respecting animal life, minimizing animal suffering to the greatest extent possible, conducting animal experiments only when necessary, and minimizing the number of experiments whenever possible. Additionally, all experiments were conducted by experienced researchers. A 1% pentobarbital sodium solution (40 mg/kg) was injected intraperitoneally to humanely sacrifice the experimental subjects.

TCGA NPC data download and analysis

We acquired and analyzed NPC data from the TCGA database. Initially, the TCGA portal was used to access transcriptome sequencing data along with clinical records related to NPC patients. Subsequently, Perl scripting facilitated data preprocessing, ultimately producing organized outputs in the form of gene matrices and clinical data files. The dataset comprises 128 samples of human nasopharyngeal epithelial tissue, comprising 12 normal samples and 116 tumor samples. Inflammation-related gene sets were curated through the GSEA website. The'limma'R package was employed to detect inflammation-associated genes showing differential expression (|log2 FC|> 1, FDR <0.05) between NPC tumor samples and normal tissue. Subsequently, we will integrate the clinical data of patients with NPC with gene matrices. This merged dataset will then be analyzed using the R software package"survival"to identify inflammation genes associated with the prognosis of NPC patients. These identified genes will be further compared to differentially expressed genes (DEGs) to identify any overlapping genes.

A Lasso regression approach was applied, using the R package "glmnet", to screen out the most informative genes and construct a robust predictive model. First, we applied Lasso regression modeling to Cox-significant genes ($p< 0.05$) and determined the optimal λ (Lambda) value through tenfold cross-validation. A Cox regression framework was applied, incorporating gene expression profiles as explanatory variables and survival metrics (futime and fustat) as outcomes, to calculate gene-specific regression coefficients. We applied L1 regularization (Lasso regression) to reduce redundant gene interference, selecting the optimal Lambda through cross-validation, and ultimately identified the key inflammation-related genes. NPC patients were classified into high-risk and low-risk groups based on the median risk score, and the assessment of the clinical risk model's predictive value was executed.

A multi-dimensional evaluation of the model was performed using risk analysis via Riskplot, overall survival (OS) analysis, receiver operating characteristic (ROC) analysis, Cox regression analysis, progression-free survival (PFS) analysis, and clinical feature correlation studies. Furthermore, analysis included the examination of distinct immune characteristics between high- and low-risk groups, encompassing cellular immunity, checkpoint gene regulation, immune function, and potential for immunotherapy response. A comprehensive literature review was conducted to collect the immune checkpoint-related gene sets used in this analysis (Hu et al. 2020). The scoring file for immunotherapy is obtained from the TIDE website. Additionally, immune cell distribution differences between tumor and normal samples in NPC were evaluated through the CIBERSORT computational framework. Furthermore, expression verification of genes in head and neck squamous cell carcinoma (HNSC) patients was performed via the GEPIA online analysis portal.

Single-cell RNA sequencing (scRNA-seq) and bioinformatics analysis

Our hospital collected both neoplastic and adjacent non-neoplastic tissue specimens from eight NPC patients who had surgical resections between 2020 and 2022. After the operation, these specimens were diagnosed and confirmed as NPC by two pathologists independently, relying on morphological and immunohistochemical findings. All patients did not receive treatment before the surgery. Post-excision, the tissue material is cryogenically treated by immersion in liquid nitrogen and held in storage at -80 °C for subsequent research use. Ethical endorsement for the study was issued by the ethics

committee at Shengjing Hospital of China Medical University, and informed consent from patients was obtained in full compliance with the Helsinki Declaration's requirements.

We selected two paired tumor tissues and their corresponding adjacent normal tissues. We isolated individual cells using standard density gradient centrifugation and conducted 10 ×scRNA-seq. The 10 Chromium Single Cell platform was employed to barcode-label cell suspensions, enabling a loading range of 300–500,000 cells. The generation of single-cell RNA sequencing libraries was performed using the Chromium Single Cell 3'v3 (1000269), 5'v2 (1000298), and J (1000230) kits, strictly adhering to the manufacturer's protocol. A unique sample index generates each sequencing library sequenced on the Illumina platform.

For preprocessing and quality control of the raw sequencing data, we utilized the R software packages Cellranger v3.0.2 and Seurat v4.0.2. Filtering criteria included the elimination of cells with Unique Molecular Identifiers (UMI) counts below 1000, fewer than 200 expressed genes, or mitochondrial gene content greater than 5%. Simultaneously, to remove potential doublets, the filtering pipeline also involved removing cells with UMI counts higher than 25,000 and genes that were detected in a cell population exceeding 5,000. The quality-filtered dataset underwent log transformation, leading to the creation of a normalized gene expression matrix.

Feature selection, dimension reduction, and clustering analysis were performed on single-cell transcriptome data using Seurat v4.0.2. Initially, we identified 2,000 genes with high variability using variance stabilizing transformation. Subsequently, dimensionality reduction and cell clustering were achieved by first executing principal component analysis (PCA), then applying tSNE. Candidate genes were filtered by setting criteria of over 25% expression prevalence and a fold change cutoff greater than 0.25. We then augmented our selection with marker gene definitions sourced from the CellMarker 2.0 database (http://bio-bigdata.hrbmu.edu.cn/CellMarker/). The annotation of cell populations was achieved applying marker genes refined with both SingleR v1.2.4 and celldex v1.2.0 R packages on the complete dataset. For subsequent Analysis, we chose cells with marker gene expression values aligned with the annotated cell types (Wang et al. 2023b).

Functional enrichment analysis of DEGs

The gene list with differential expression obtained from TCGA was compared to the DEGs of macrophages obtained through scRNA-seq Analysis. Biological functions of macrophages in both tumor and normal nasopharyngeal epithelial samples were analyzed through functional enrichment, applying Gene Ontology (GO) and the Kyoto Encyclopedia of Genes and Genomes (KEGG) databases for pathway investigation. Subsequently, we conducted additional investigations into the mechanisms that drive macrophage differentiation in tumor tissues using the resources available on the String and ChIPBase v3.0 websites (Yang et al. 2022).

Flow cytometry

We performed mechanical dissociation of both normal and tumor tissue, which were obtained from NPC patients. Following enzymatic digestion with Sigma enzyme (5401020001), the tissues were strained using a 40 μm nylon mesh and converted into single-cell suspensions. Immunostaining was conducted overnight at 4 ℃ on a population of macrophage-like neuronal cells (MNT) using an APC-conjugated antibody against CD68 (#MA5-23616, Thermo Fisher) and a FITC-conjugated antibody against TUBB3 (#MA1-19582, Thermo Fisher), targeting the respective neurotubule-associated proteins. Detection of neuron-like macrophages of nude mice was achieved through flow cytometry. Overnight staining was performed using antibodies F4/80-APC (#17–4801-82, Thermofisher) and TUBB3-FITC (#MA1-19582, Thermofisher). For cell analysis, the FACS Aria II Cell Sorter (BD Biosciences) facilitated flow cytometry, followed by data evaluation through TreeStar's FlowJo software. The FSC/SSC gating strategy divided cell populations into four quadrants (Q1-Q4) based on cell size and granularity: CD68 + cells: Macrophages, TUBB3 + cells: Neuron-like differentiated macrophages, $F4/80^+$ cells: Macrophages. Each of the above materials was procured from its respective vendor—Sigma and Thermofisher.

Cell culture

The following cell lines were obtained from Cellverse Co., Ltd. (Shanghai, China Human NPC cells

(HK-1) (iCell-h367), Normal human nasal epithelial cells (NP69) (iCell-h431). The following macrophage cell lines were obtained from Biobw:, human macrophages (bio-53611), and mouse bone marrow-derived macrophages (BMDMs, bio-81930) from Biobw. The normal human nasal epithelial cells (NHNECs) (tings-95173) were purchased from Hefei All Things Biotech Co., Ltd. The culture conditions included DMEM medium (11965092, Gibco) with additives: 20% fetal bovine serum (FBS, 12483020, Gibco), 2 mM L-glutamine (A2916801, Gibco), plus penicillin (100 U/mL) and streptomycin (100 μg/mL, Gibco, 15140148). A CO_2 incubator set at 37 °C was used to sustain the cultured cells. Thermofisher served as the provider for every material referenced above.

Single-cell suspensions were generated from bone marrow cells extracted from the tibias of male C57BL/6 nude mice aged 6–8 weeks and weighing 22–25 g. Macrophage differentiation was induced by culturing the cells for 7 days in DMEM/F12 medium containing 10% heat-inactivated fetal calf serum (FCS) and 50 ng/mL of recombinant mouse macrophage colony-stimulating factor (M-CSF) (Gibco, PMC2044). MNTs was further promoted by treating BMDMs with TGF-β1 at a concentration of 5 ng/mL over five days, followed by culturing them in 10% (v/v) LLC-CM (Lewis lung carcinoma-conditioned medium) for a period of seven days (Tang et al. 2022).

Co-culture of cells *in vitro*

NP69 or HK-1 cells were co-cultured with human macrophages (1:5) at 37 °C and 5% CO2 for one week. The upper well of the Transwell plate (CLS3412, Corning) was populated with NP69 and HK-1 cells, whereas human macrophages were seeded into the lower well for co-cultivation. A 0.4 μm membrane separates NPC cells (NP69) or HK-1 cells from human macrophages, allowing only soluble molecules to diffuse across. After one week, retrieve the resident macrophages from the basement to conduct further experiments. Additionally, HK-1 cells transfected with human macrophages were co-cultured. The cells were divided into four groups based on the type of transfection of human macrophages: control group, sh-NC group, sh-TREM2 group, and sh-APOE group.

Cell transfection

Lentiviral transfection was employed to establish the subsequent cell lines: human macrophages with silenced *TREM2* (sh-TREM2) and their respective control (sh-NC), mouse BMDMs with silenced *TREM2* (sh-TREM2) and their respective control (sh-NC), human macrophages with silenced *APOE* (sh-APOE) and their respective control (sh-NC), and human macrophages with silenced *APOE* and overexpressed *TREM2* (sh-APOE + oe-TREM2) and their respective control (sh-APOE + oe-NC). Shanghai Hanheng Biotechnology Co., Ltd. (Shanghai, China) provided all *TREM2* silencing and overexpression plasmids along with their corresponding lentiviruses, as well as the *APOE* silencing constructs and related viral vectors. 293 T cells (bio-73410, Biobw) were transfected with lentiviral pHBLuc constructs, including sh-NC, sh-TREM2, and sh-APOE plasmids. Following validation, expansion, and purification steps, the lentiviruses were packaged for subsequent use. Cell transfection via lentiviral vectors involved plating 500,000 cells in each well of a 6-well dish. Transduction was carried out at 70–90% cell confluency by introducing lentivirus (MOI = 10; working titer ≈5 $\times 10^6$ TU/mL) and polybrene at 5 μg/mL (TR-1003, Merck) into the culture environment. Four hours post-transfection, an equivalent volume of medium was introduced to reduce the concentration of polybrene, followed by a complete medium change at the 24-h mark. Stably transfected cells were enriched using 1 μg/mL puromycin (A1113803, Thermofisher) after a 48-h transfection phase. A viral dose of MOI 10 was used to introduce lentiviruses into human and mouse BMDMs, with 5 μg/mL puromycin (A1113803, Gibco) added during the process. shRNA transfected with silencing sequence see (Table S1).

RT-qPCR

First, separate total RNA from cells and tissues. Tissue samples were homogenized in TRIzol reagent (10296010, Thermo Fisher) at 1 mL per 100 mg, followed by the addition and thorough mixing of 200 μL chloroform. After centrifugation at 12,000 g for 10 min at 4 °C, the upper aqueous layer was isolated and 500 μL of isopropanol was added to facilitate RNA precipitation. Two rinses were carried out using 75% ethanol before RNA was rehydrated

in DEPC-treated water (10–30 μL, R0021, Beyotime), followed by quantification with a Nanodrop device (3300 model, Thermofisher). Reverse transcription of 1 μg total RNA was achieved with the TaqMan Reverse Transcription Kit (Thermofisher, N8080234). PCR amplification utilized the PowerUp SYBR Green PreMix Kit (A25741, Thermo Fisher), and *GAPDH* was adopted as the reference gene for relative quantification using the $2^{-\Delta\Delta CT}$ technique. The primer sequences are listed in (Table S2) (Franke et al. 2021; Peng et al. 2020).

Western blot

RIPA lysis buffer, including 4% protease inhibitor (P0013B, Beyotime), was used to lyse cells and tissues for total protein extraction at 1 mL per 100 mg, in accordance with manufacturer recommendations. The BCA assay kit (P0010S, Beyotime) was utilized to quantify protein concentrations, and equivalent protein amounts were loaded onto SDS-PAGE gels for electrophoretic separation. The separated protein bands were subsequently migrated to a polyvinylidene fluoride membrane (FFP24, Beyotime) by applying the wet transfer protocol. TBST buffer containing 5% skim milk (P0216-300 g, Beyotime) was used to block the membrane for 1 h at room temperature before an overnight incubation at 4 ℃ with the primary antibody. Employed in the study were these antibodies: anti-TUBB3-50 kDa (#MA1-118, 1:500, Thermo Fisher), anti-*TREM2*−25 kDa (#PA5-87933, 1:1000, Thermo Fisher), anti-*APOE*−34 kDa (#701241, 1:1000, Thermo Fisher), and anti-GAPDH-36 kDa antibody (#SAB4300645, 1:1000, Sigma). The purchase mentioned above was made from Thermofisher and Sigma. Following the TBST washing, the samples were incubated with a horseradish peroxidase-labeled goat anti-rabbit secondary antibody (A0208, 1:1000, Beyotime) at room temperature for one hour. Subsequently, the ECL chemiluminescence detection reagent (P0018 FS, Beyotime) was introduced, and images were acquired through the ChemiDoc XRS + chemiluminescence system (Bio-Rad). Protein levels were quantified via ImageJ analysis, involving grayscale calculation and ratio determination relative to the internal reference protein GAPDH.

Cell fluorescent staining

Each well of the 12-well culture plate, treated with 0.01% poly-L-lysine (P8920, Sigma), received a seeding density of 2000–3000 cells. Cells were immobilized applying paraformaldehyde (PFA) at a concentration exceeding 4%, followed by PBS rinsing, 0.5% Triton-X 100 (T8787, Sigma) permeabilization, and blocking with 3% BSA (ST025, Beyotime) at room temperature for 1 h before overnight primary antibody incubation at 4 °C. Utilized were the subsequent antibodies: anti-human/mouse TUBB3 (#MA1-118, 1:50 dilution, Thermofisher), anti-human CD68 (#14–0689-82, 1 μg/mL concentration, Thermofisher), anti-human NeuN (#702022, 1:50 dilution, Thermofisher), and anti-mouse F4/80 (#14–4801-82, 5 μg/mL concentration, Thermofisher). A series of three PBS rinses was performed on the cells the following day. Subsequent incubation with the secondary antibody (#A0208, Beyotime) was conducted in darkness at room temperature for two hours. Re-stain the cell nuclei using DAPI dye (62247, Thermofisher). Images were obtained with a fluorescence microscope (Olympus X73, Japan), followed by analysis of signal intensity using Image-J. Reagents listed earlier were sourced from Sigma, Thermofisher, and Beyotime. The fluorescence signal statistics were evaluated from five distinct dimensions (Hong et al. 2022).

Animal experiments *in vivo*

The study involved C57BL/6 male nude mice (athymic), aged 6 to 8 weeks, with body masses ranging from 22 to 25 g. The mice were procured from Hunan Slacc Jingda Experimental Animal Co., Ltd., in Changsha, China. The supplier holds an Experimental Animal Production License (SCXK-2016–0002). Within SPF-certified animal housing, nude mice were singly caged and underwent a one-week pre-experimental adaptation exposed to 24-h light–dark alternation to promote feeding habituation. Nude mice underwent health and condition checks before the experimental process began. The Animal Ethics Committee of Shengjing Hospital of China Medical University authorized all animal-related protocols, which were implemented in compliance with local ethical guidelines for animal experimentation.

Before commencing the Experiment, the nude mice were randomly allocated into three groups, each containing ten mice. Subsequently, all nude mice were intraperitoneally injected with diphtheria toxin (150 ng per mouse, dissolved in saline) from Sigma (D0564) to selectively deplete macrophages. Next, all nude mice were subcutaneously injected with 4×10^6 HK-1 cells to establish a subcutaneous tumor model. Afterward, after receiving 2×10^6 intravenously administered BMDMs, either with or without transfection, the nude mice were separated into control, sh-NC, and sh-TREM2 groups for further analysis. According to previous reports, on the 20 th day after the Experiment commenced (Tang et al. 2022), The number of licking and withdrawal actions by the nude mice should be recorded, alongside the observation of pain response levels among different groups of nude mice. Following that, a 1% solution of pentobarbital sodium (40 mg/kg) was intraperitoneally injected into all nude mice to induce anesthesia. Euthanasia was then conducted through cervical dislocation. Subcutaneous tumors were excised and preserved in 4% PFA for 48 h, then subjected to dehydration and embedding procedures, followed by sectioning into 5 μm paraffin slices.

The presence of neuron-like macrophages in the tumor tissue was subsequently determined using immunofluorescence staining and flow cytometry experiments. The staining steps in organisms for immunofluorescence are slightly distinct from those used in cells. In summary, the prepared tissue sections were fixed with 1% PFA and heated for 1 h to extract antigens. Antigen extraction was carried out using Tris–EDTA buffer (ST725, Beyotime) at a temperature of 100 °C. Permeabilization with 0.5% Triton X-100 for 10 min was followed by a 1-h blocking incubation in 3% BSA dissolved in PBS. They were kept at 4 °C throughout the night to complete the incubation phase. The subsequent steps of processing are identical to the previous ones. The fluorescent counting results are from five perspectives (Ding et al. 2021).

Statistical examination

Statistical evaluation of the dataset was conducted using SPSS 21.0 software (IBM, USA), with quantitative values expressed as mean ± SD. Two-group comparisons utilize t-tests, in contrast to one-way ANOVA, which handles comparisons across several groups. Repeated measures ANOVA serves the purpose of comparing data captured at different time points, thereafter conducting Tukey's post-hoc analysis. The thresholds for statistical significance are represented by asterisks: $*p < 0.05$ for modest, $**p < 0.01$ for moderate, and $***p < 0.001$ for high significance.

Results

Inflammation and gene expression in NPC

As a fundamental immune function, inflammation is initiated in response to potentially harmful stimuli, including infectious organisms, noxious chemicals, cellular impairment, and ionizing radiation. Inflammatory responses are typically marked by erythema, edema, elevated temperature, nociception, and impaired tissue functionality. Extended periods of inflammatory activity can predispose individuals to various chronic inflammatory conditions. Cancer patients often exhibit chronic inflammatory states, which are associated with aberrant neural responses such as increased neuronal excitability, reorganization of neural signaling routes, and other disease-related neural changes (Yim et al. 2022). Previous research has indicated that patients diagnosed with NPC commonly undergo intense and localized pain (Huang et al. 2022). This pain impacts the patient's daily life; however, no existing literature explains its underlying mechanism.

To investigate the mechanisms underlying pain response in patients with NPC, we initially obtained transcriptome sequencing data of tumor tissues from NPC patients, as well as adjacent normal tissues, from the TCGA database. Upon completion of dataset refinement and differential gene expression evaluation, 1885 DEGs were found to distinguish NPC tumor tissues from healthy nasopharyngeal epithelial cells. Among them, 1,548 genes showed up-regulation, while 337 genes exhibited down-regulation (Fig. 1A). A total of 92 inflammation-correlated DEGs were discovered in NPC tumor tissues, based on the gene set pertaining to inflammation downloaded from the GSEA website. Among them, 83 genes were upregulated, while 9 genes were downregulated (Fig. 1B). We identified

five inflammation-related genes (Fig. 1C) associated with prognosis in patients with NPC by merging clinical data. A set of three overlapping genes—*LCK*, *ITGA5*, and *TLR2*—was obtained by cross-analyzing the inflammation-related DEGs and the prognostically relevant inflammatory gene set (Fig. 1D). The expression of these three common genes is increased in patients with NPC. Additionally, increased *LCK* expression tends to indicate a more favorable prognosis in patients suffering from NPC. Conversely, an increased expression of *ITGA5* and *TLR2* is associated with a higher risk of unfavorable patient outcomes (Fig. 1E-F).

Next, randomized allocation of patients into training and testing datasets is applied to mitigate overfitting during model development. We constructed a Lasso regression model and selected six genes demonstrating the best simulation effect for

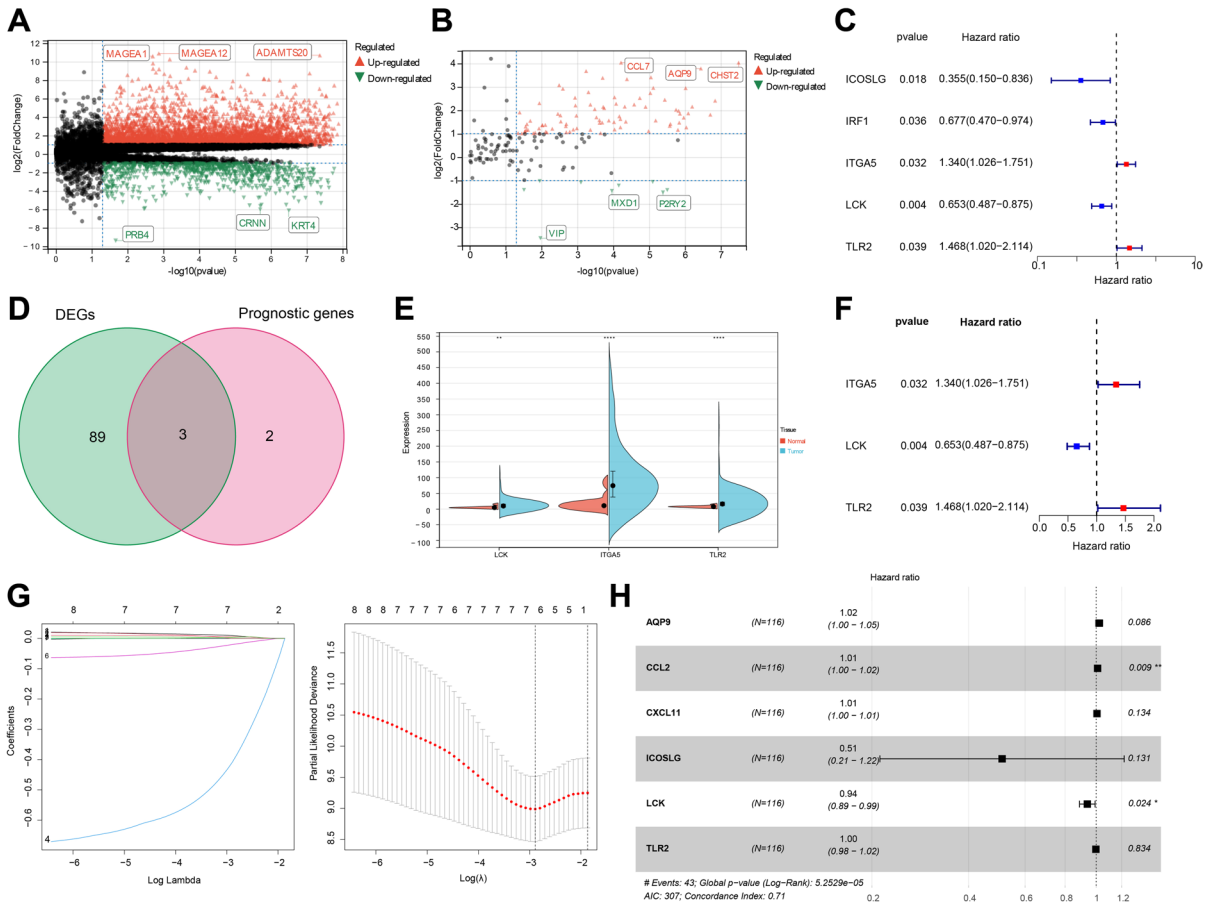

Fig. 1 Differential Analysis based on the TCGA Database and Construction of a Prognostic Risk Model based on Inflammation-related Marker Genes. Note: (**A**) Volcano plot showing differential genes between normal tissue ($n = 12$) and cancer tissue ($n = 116$) in NPC patients from TCGA database; (**B**) Volcano plot showing differential inflammation-related genes between normal tissue ($n = 12$) and cancer tissue ($n = 116$) in NPC patients from TCGA database; (**C**) Forest plot of univariate COX analysis on inflammation-related genes based on the TCGA database (5 prognosis-related genes are shown, represented by red for positive correlation and blue for negative correlation); (**D**) Venn diagram showing the overlap between inflammation-related differential genes and inflammation-related prognostic genes; (E) Expression levels of *LCK*, *ITGA5*, and *TLR2* in normal tissue ($n = 12$) and cancer tissue ($n = 116$) of NPC patients from TCGA database, $*p < 0.01$, $**p < 0.0001$; (**F**) Correlation between *LCK*, *ITGA5*, *TLR2*, and prognosis in NPC patients; (**G**) Distribution plot of Lasso coefficients (each line represents a gene, and the vertical coordinate at the end of the line represents the gene's coefficient) and Lasso regression model plot (the vertical coordinate represents cross-validation error, and the number of genes corresponding to the point of minimum error is the optimal model); (**H**) Forest plot of COX risk scoring model (displaying model genes and their risk coefficients)

building the model (Fig. 1G). Subsequently, we constructed a Cox proportional hazards model using the'Survival'package to analyze the gene expression data from the training group. The model was built for genes that were associated with Lasso regression. It provided risk coefficients for the genes and risk scores for each sample. Following the construction of the model, we derived a prognostic risk score model consisting of six genes: *AQP9*, *CCL2*, *CXCL11*, *ICOSLG*, *LCK*, and *TLR2*. The risk coefficients for these genes are illustrated in (Fig. 1H).

Conclusive evidence from our investigation indicates that inflammatory gene expression is markedly enhanced in tumors derived from NPC patients.

Risk stratification and immune landscape in NPC

Through application of the model, two prognostic groups—high-risk and low-risk—were identified among NPC patients. The mortality rate of NPC patients in high-risk areas is higher (Fig. 2A). The OS duration of NPC patients differs significantly between those in the high-risk group and those in the low-risk group, as revealed by survival analysis (Fig. 2B). All area under the curve (AUC) metrics derived from the ROC analysis of 1–3-year survival in NPC patients are greater than 0.7, confirming the model's precise predictive capability (Fig. 2C). Independent prognosis analysis results indicate that gender is an important prognostic factor in NPC patients. Cox regression

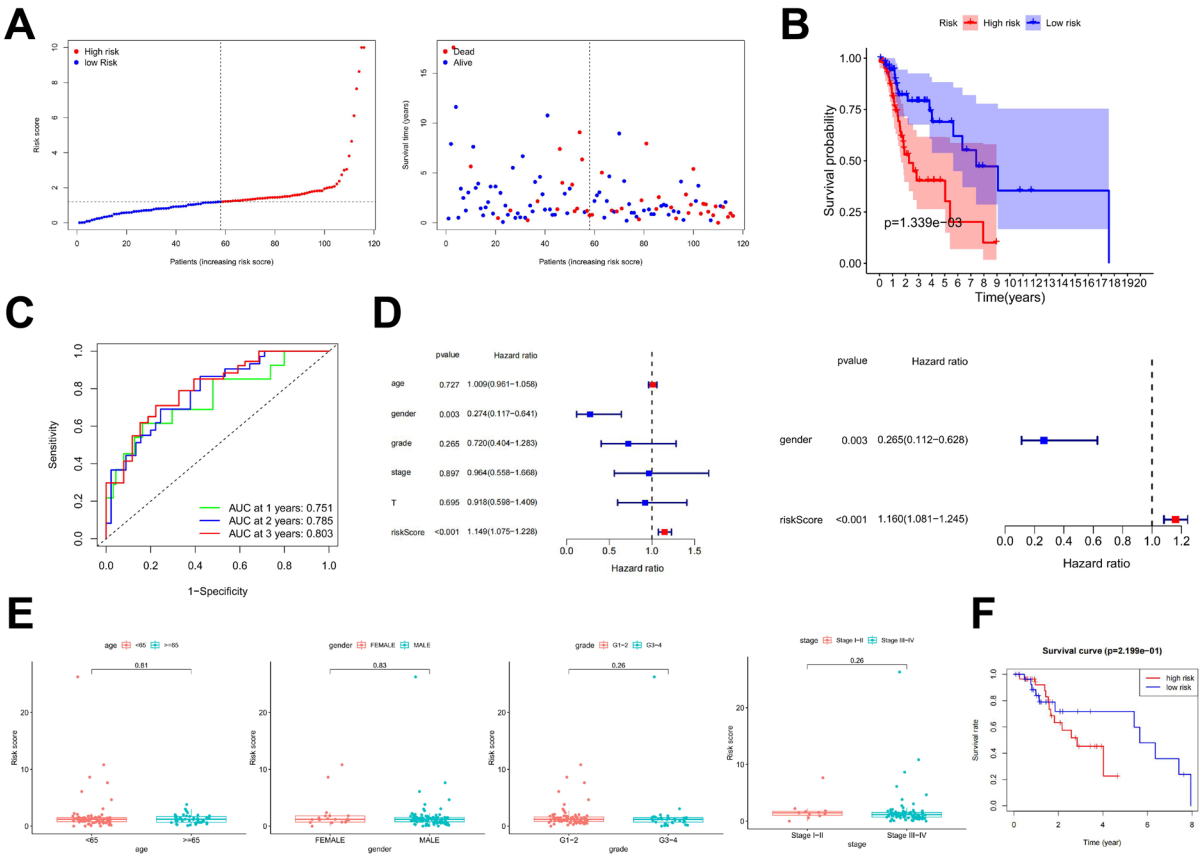

Fig. 2 Performance Evaluation of the Prognostic Risk Score Model based on Inflammatory Marker Genes. Note: (**A**) Risk curve (left) and risk heatmap (right) between high and low-risk groups of NPC patients in TCGA training set ($n = 58$); (**B**) OS analysis between high and low-risk groups of NPC patients in TCGA training set ($n = 58$); (**C**) ROC curve analysis predicting 1–3 year prognosis of NPC patients based on risk values in TCGA training set ($n = 58$); (**D**) Univariate analysis (left) and multivariate analysis (right) of prognosis-related factors predicting NPC patient prognosis in TCGA training set ($n = 58$); (**E**) Correlation analysis of NPC patient risk values and clinical characteristics in TCGA training set ($n = 58$); (**F**) OS analysis between high and low-risk groups of NPC patients in TCGA test set ($n = 58$)

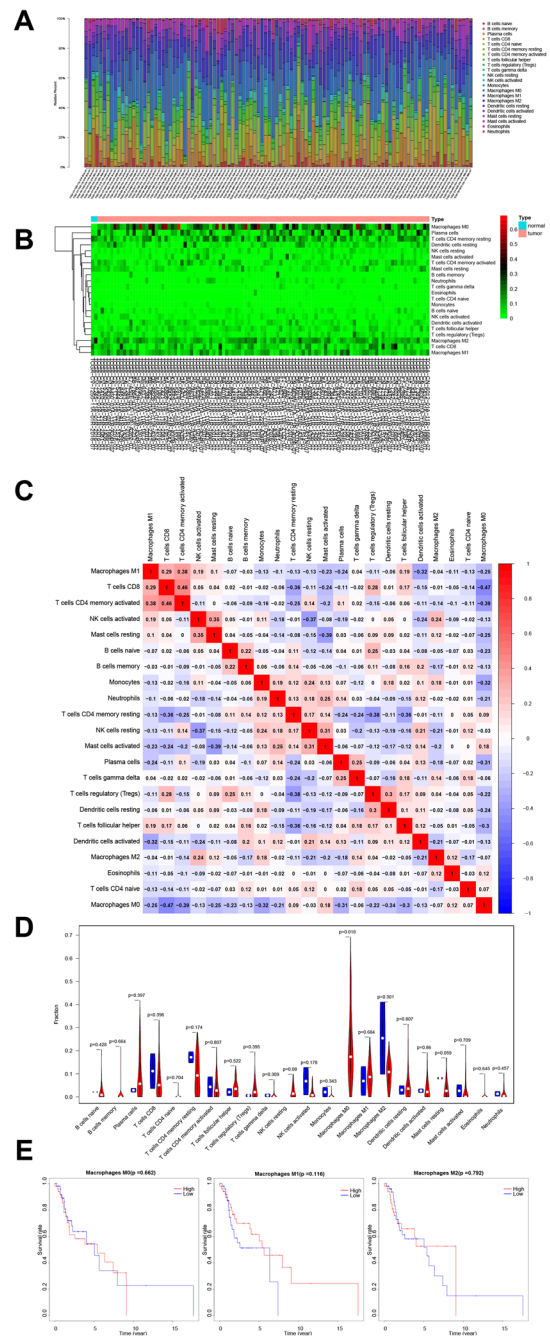

Fig. 3 Analysis of Immune Cell Infiltration in NPC Tumor Tissue based on the TCGA Database. Note: (**A**) Stacked column chart showing the composition of immune cells in normal tissue ($n = 12$) and tumor tissue ($n = 116$) of NPC patients from TCGA database; (**B**) Heatmap showing the composition of immune cells in normal tissue ($n = 12$) and tumor tissue ($n = 116$) of NPC patients from TCGA database; (**C**) Heatmap showing the correlation of immune cells between normal tissue and tumor tissue of NPC patients from TCGA database; (**D**) Violin plot showing the differential content of immune cells between normal tissue (blue) and tumor tissue (red) of NPC patients from TCGA database; (**E**) Correlation analysis between different macrophage content and OS time of NPC patients in tumor tissue ($n = 116$)

analysis—both univariate and multivariate—demonstrates a gender-associated hazard ratio of 0.274 (95% CI: 0.117–0.641, $p = 0.003$), clearly lower than 1, thereby indicating a survival benefit linked to one gender (e.g., females), depending on the variable coding. Meanwhile, the risk score's hazard ratio (HR = 1.149, 95% CI: 1.075–1.228, $p < 0.001$) is greater than 1, demonstrating that a higher risk score is significantly associated with worse prognosis (Fig. 2D).

Nevertheless, the Analysis uncovered no discernible correlation between the clinical symptoms of patients with NPC and the levels of inflammatory risk, as illustrated in Fig. 2E. Furthermore, the Test group's gene expression signatures served as the foundation for a predictive risk model used to examine NPC patient survival time. The analysis indicated that the prognosis was notably less favorable for patients within the high-risk cohort (Fig. 2F).

Furthermore, additional investigations were carried out to evaluate the immune cell variations between normal and tumor tissues in patients with NPC (Fig. 3A). The outcomes of the study suggest that the majority of individuals suffering from NPC display heightened levels of three classifications of immune cells within tumor tissues: Macrophages M0 (M0 macrophages), Plasma cells, and T cells CD4 Memory Resting (resting memory state of CD4 T cells). However, there is no substantial correlation observed among these three cell types (Fig. 3B-C). Our Analysis revealed that, compared to normal tissues, the tumor tissues of NPC patients exhibited an overall increase in the content of most immune cells, except'Monocytes'and'Macrophages M2.'Notably, there was an increase in the content of'Macrophages M0'(Fig. 3D). In Fig. 3E, we analyzed the correlation between different macrophage subtypes (M0, M1, M2) and NPC patients'OS. The results indicate that M1 macrophage (Macrophages M1) enrichment is associated with higher survival rates (p = 0.116), although it did not reach statistical significance. Compared to M0 and M2 macrophages, M1 macrophages are key indicators of inflammatory responses and typically play a role in promoting

inflammation and enhancing anti-tumor immunity. Therefore, our results suggest that M1 macrophage enrichment may have a potential protective effect on NPC patient survival. In addition, the presence of"M1 macrophages","neutrophils","CD4 memory T cell activation", and"T follicular helper cells"is strongly associated with tumor malignancy in patients with NPC (Figure S1A).

In summary, our study suggests that while most inflammation-related genes and immune cell abnormalities are associated with poor prognosis in NPC patients, M1 macrophage enrichment may have a protective effect on survival. Such evidence points to a bidirectional role for macrophages in the NPC context, with future studies required to unravel the specific mechanisms at play.

Macrophages, inflammation risk, and immune therapy in NPC

To gain deeper insights into how macrophages relate to high- and low-risk NPC patient groups, we conducted a comparative assessment of immune-related functionalities and the immune microenvironment. Differential abundance of immune cells was detected between the two NPC patient cohorts distinguished by risk level. Patients in the high-risk category showed significantly greater infiltration of'resting memory state of CD4 T cells', M0 macrophages, and activated hypertrophic cells. Conversely, patients in the low-risk group exhibited significantly enhanced levels of six immune cell types, particularly Naive B cells, plasma cells, and regulatory T cells (Fig. 4A). However, the overall quantities of immune and stromal cells appeared similar in both groups, showing no statistically significant variation (Fig. 4B).

Our results demonstrate a decrease in the expression of immune checkpoint-related genes in tumor cells from the high-risk group compared to the low-risk group (Fig. 4C). This finding aligns with the overall downregulation of immune checkpoints, as shown in Fig. 4D. Building upon this phenomenon, we conducted a more in-depth analysis of the effectiveness of immune therapy in two distinct patient populations. However, no significant differences emerged between the groups in the analysis, potentially resulting from reduced cytotoxic activity of cells in the high-risk cohort (Figure S1B, Fig. 4D). Our Analysis revealed a negative correlation between the stem cell traits of tumor cells in patients with NPC and the risk of inflammation (Fig. 4E). In addition, the GSEA analysis showed a notable enrichment of genes related to functions like"translation initiation factor activity","plasminogen activation", and"pre-initiation complex"(Fig. 4F) in the high-risk group. These functions are known to be associated with generating the pain response (Yousuf et al. 2021). Additionally, drug sensitivity in cancer therapy appears to be linked with the expression patterns of six genes utilized in the formulation of risk assessment models (Figure S2). There are positive correlations between *LCK*, *AQP9*, and various tumor therapeutic drugs.

Recent research indicates that macrophages in tumor tissues can differentiate and transform into neuron-like macrophages through MNT. This result suggests their involvement in the development and propagation of pain reactions observed in cancer patients (Tang et al. 2022). An elevated presence of M0 macrophages was detected in high inflammation–risk NPC individuals, emphasizing their pivotal involvement in mediating localized pain responses in these patients.

Macrophage differentiation in NPC tissues: a single-cell analysis

We utilized single-cell sequencing of malignant and normal nasopharyngeal tissues from NPC patients to evaluate the proposed link between macrophages and localized pain. After merging the datasets with the Seurat package, we conducted an initial analysis to assess the number of genes (nFeature_RNA), mRNA molecule count (nCount_RNA), and the proportion of mitochondrial genes (percent.MT) across all cells within the scRNA-seq dataset. The outcomes suggested that most cells exhibited nFeature_RNA levels below 8000, nCount_RNA levels below 4000, and a percentage of MT below 20% (Figure S3A). Low-quality cells were filtered out, resulting in an expression matrix encompassing 25,997 genes across 27,884 cells. Meeting the set criteria involved nFeature_RNA counts ranging from 200 to 5000 and keeping the percent.MT counts below 20%. The results of the correlation analysis revealed a correlation coefficient (r) of 0.46 between nCount_RNA and percent.MT, and a correlation coefficient (r) of 0.66 between nCount_RNA and nFeature_RNA (Figure S3B). The data obtained post-filtering demonstrated sufficient

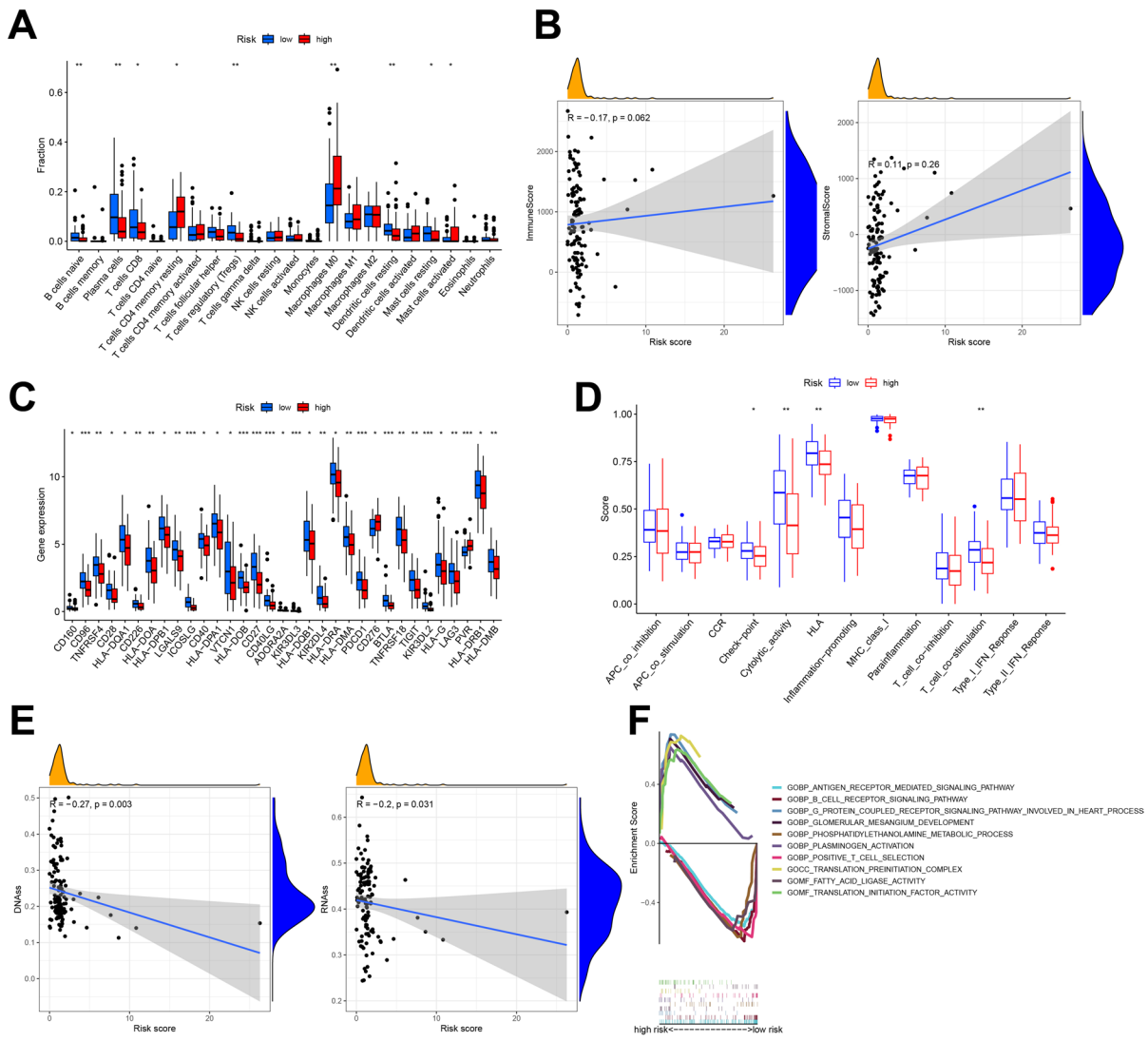

Fig. 4 TME in NPC Tumor Tissue based on Different Inflammation Risk Groups from the TCGA Database. Note: (**A**) Analysis of differential immune cell infiltration between high-risk ($n = 58$) and low-risk ($n = 58$) groups of NPC patients in the TCGA database; (**B**) Correlation analysis between risk values and the total amount of immune cells (left) and stromal cells (right) in NPC tumor tissue from the TCGA database; (**C**) Analysis of differential immune checkpoint expression between high-risk ($n = 58$) and low-risk ($n = 58$) groups of NPC patients in the TCGA database; (**D**) Analysis of differential immune function between high-risk ($n = 58$) and low-risk ($n = 58$) groups of NPC patients in the TCGA database; (**E**) Correlation analysis between risk values and tumor stem-like characteristics in NPC tumor tissue from the TCGA database; (**F**) GSEA analysis of functional enrichment of differential genes in NPC tumor tissue between high-risk ($n = 58$) and low-risk ($n = 58$) groups. * denotes comparison between groups, $*p < 0.05$, $**p < 0.01$, $***p < 0.001$

quality to support subsequent computational or biological investigations.

An in-depth evaluation of the post-filtered cellular dataset was undertaken, and genes displaying the highest expression variability were extracted through rigorous screening. Subsequently, the downstream analysis focused on the variance of the top 2000 genes (Figure S3D). A linear dimensionality reduction was achieved via PCA, and the major gene expression relationships within PC_1 to PC_6 were visualized using a heatmap, as presented in Figure S3C.

Batch correction was carried out using the harmony package, aiming to streamline future data interpretation and analysis (Figure S3E). Additionally, we utilize ElbowPlot to standardize and sort principal components (Figure S3F). The data suggest that PCs 1 through 50 retain critical patterns embedded in the most variable genes, confirming their utility for further analytical exploration. Therefore, t-SNE was applied to perform nonlinear dimensionality reduction using the leading 50 PCs. The clustering results at various resolutions were then presented using the cluster package (Figure S4).

Based on the clustering results, a resolution of 0.4 was chosen for clustering, which resulted in a total of 18 clusters. A noticeable distinction in cell clustering was observed between normal nasal epithelial tissue and tumor tissue (Fig. 5A). Using clustering, it was observed that clusters 1–4 were predominantly present in normal tissue, whereas clusters 0, 5–6, and 8–9 were predominantly found in tumor tissue (Fig. 5B). Based on the expression patterns of marker genes, we manually annotated 18 clustering clusters and identified four cell types: epithelial cell, T cell, B cell, and macrophage (Fig. 5C). Clusters 0, 10, and 16 are labeled as B cells, while clusters 5–6 and 8 are labeled as T cells. Cluster 9 is labeled as macrophages, and the rest are labeled as epithelial cells. It is important to note that, despite cluster 0 and cluster 10 being annotated as B cells, they are displayed in different colors in the annotation results. It indicates the existence of two distinct B cell subpopulations in the tumor tissues of NPC patients. In our study, cluster 9 was annotated as macrophages, indicating their enrichment in NPC tumor tissues.

Our findings indicate that normal tissues consist primarily of epithelial cells with a lower concentration of immune cells, whereas tumor tissues exhibit a substantial rise in immune cell population (Fig. 5D). Taken together, these findings demonstrate that macrophages are significantly enriched in the nasopharyngeal tumor tissues of NPC patients.

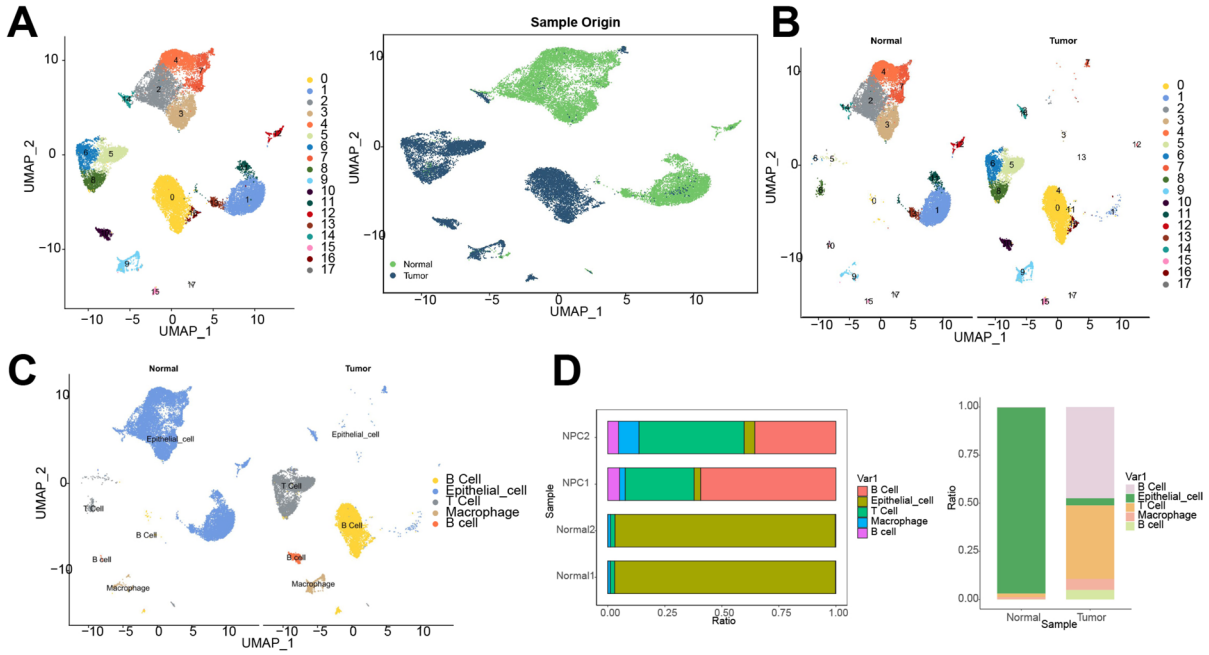

Fig. 5 UMAP Cell Clustering and Annotation of scRNA-seq Data. Note: (**A**) Visualization of UMAP clustering results, where each color represents a cluster, and the right plot shows the cell aggregation and distribution of samples from the Normal and Tumor groups; (**B**) Cell aggregation and distribution of samples from different sources; (**C**) Visualization of cell annotation results based on UMAP clustering, where each color represents a cell population; (**D**) Percentage of different cell populations in samples from the Normal and Tumor groups

MNT cell differentiation in NPC tissues and co-culture model

Recent studies indicate that macrophages in tumor tissues can differentiate into neuron-like cells, thereby acquiring the ability to mediate pain responses (Tang et al. 2022). Previous studies have revealed that MNT cells within tumor tissues frequently exhibit the expression of the TUBB3 protein, which is linked to neural differentiation (Tang et al. 2022). To further confirm the existence of MNT cells in NPC tumor tissue, we initially analyzed the levels of TUBB3 protein expression in macrophages present within the nasopharyngeal epithelial tumor tissue of NPC patients. An elevated number of TUBB3 + macrophages were observed in NPC tumor tissue as revealed by immunofluorescence and flow cytometry analyses (Fig. 6A-B). Simultaneously, we observed a substantial increase in TUBB3 protein expression in tumor tissue compared to normal tissue (Fig. 6C).

Afterward, an *in vitro* co-culture system was established to simulate the cellular interaction between macrophages and NPC cells. The outcomes demonstrated that co-culturing with human NPC cells, HK-1, resulted in a substantial increase in TUBB3 + cells in macrophages. Compared to co-culturing with normal human nasal epithelial cells NP69, the number of TUBB3 + cells in macrophages elevated after co-culturing with human NPC cells HK-1 (Fig. 6D-E). Furthermore, our immunofluorescence staining experiments revealed the existence of NeuN + macrophages in the HK-1 group, whereas none were observed in the NP69 group (Fig. 6F).

To summarize, we believe that MNT cells are also present in NPC, and their differentiation is caused by tumor cells.

TREM2's role in macrophage to MNT cell transformation in NPC

For a more detailed understanding of how macrophages are converted into MNT cells in NPC, we cross-examined DEGs derived from TCGA data with those extracted from NPC patient-derived macrophages. In total, we identified 42 overlapping genes (Fig. 7A). Subsequently, a total of 42 shared genes were subjected to functional annotation through GO and KEGG enrichment assessments. The outcomes of the GO analysis illustrate that these genes are primarily involved in certain functions across different categories. Specifically, in terms of biological processes, these genes are mainly associated with functions like"Granulocyte chemotaxis","Granulocyte migration", and"Cell chemotaxis". In terms of cellular components, the enrichment is observed in functions such as"External side of the plasma membrane,""Collagen-containing extracellular mat rix,"and"Chylomicron."Regarding molecular functions, the enriched functions include"Cytokine binding","Immune receptor activity", and"Polyol transmembrane transporter activity"(Fig. 7B). These functions are all related to the inflammatory response.

The results of the KEGG analysis revealed an unexpected finding that *TREM2*, *FCGR3 A*, and *FCGR3B* were enriched in the"Osteoclast differentiation"signaling pathway (Fig. 7C). The GEPIA database was employed to examine gene expression variations, applying precise selection criteria (log2 FC ≥ 2, p-value ≤ 0.001) in order to highlight key genes. The results showed that only *TREM2* met the selection criteria, while *FCGR3 A* and *FCGR3B* did not, leading us to prioritize *TREM2* for further investigation in subsequent experiments. This result suggests a potential association between these three genes and the neuronal-like differentiation of macrophages. Previous studies have consistently demonstrated an upregulation of *TREM2* in various disease models. Furthermore, expression of *TREM2* correlates with the degree of cellular differentiation, chronic inflammation, and pain response (Do et al. 2022; Cosma et al. 2023; Wu et al. 2023). This result is consistent with our analysis results (Fig. 7D). Hence, we hypothesize that *TREM2* could serve as a crucial gene for differentiating macrophages into MNT cells.

We proceeded by evaluating the *TREM2* expression in nasopharyngeal epithelial tissue samples from both healthy individuals and NPC patients' tumors. Compared to normal tissue, the level of *TREM2* is substantially higher in the tumor samples of individuals with NPC (Fig. 7E-F). We detected high expression of *TREM2* in macrophages following stimulation by CNE2 cells, as observed through co-culture (Fig. 7G-H). To investigate the role of *TREM2* as a crucial gene in converting macrophages into MNT cells, we conducted transfection of macrophages with a lentiviral transduction technique using custom-designed *TREM2* shRNA sequences for targeted

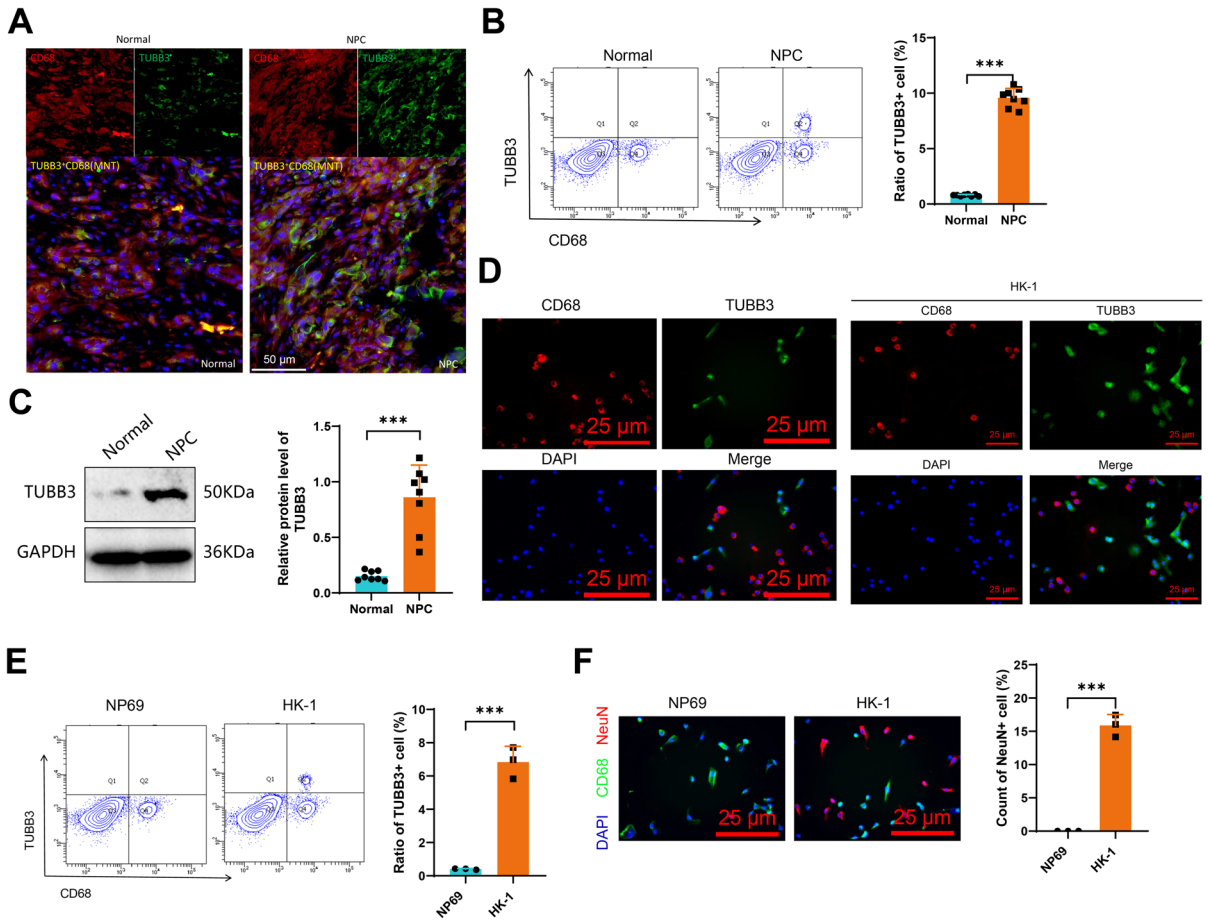

Fig. 6 Validation of the Experiment Inducing Macrophage Differentiation into MNT in NPC through Immunofluorescence Staining and Flow Cytometry. Note: (**A-B**) Immunofluorescence staining and flow cytometry experiments were conducted to detect the quantity of TUBB3 + macrophages in NPC tumor tissue ($n = 6$, Scale bars = 50 μm). Red represents $CD68^+$ macrophages (1 μg/mL), green represents $TUBB3^+$ cells (1:50), and yellow represents $TUBB3^+$ CD68 macrophages; Forward scatter (FSC) and side scatter (SSC) gating strategy was used to classify cell populations into four quadrants (Q1-Q4) to distinguish cell size and granularity. $CD68^+$ cells: Macrophages. $TUBB3^+$ cells: Neuron-like differentiated macrophages; (**C**) Western blot experiment was conducted to detect the expression level of TUBB3 protein in NPC tumor tissue ($n = 6$); (**D-E**) Immunofluorescence staining and flow cytometry analysis to detect the number of TUBB3 + macrophages after co-culture with NP69 or HK-1 cells. Red represents CD68 + macrophages (1 μg/mL), green represents $TUBB3^+$ cells (1:50), and blue represents DAPI (Scale bars = 25 μm); (**E**) Scatter plot showing the expression of neural differentiation-related genes in different cell populations. Darker red indicates higher average expression levels. Forward scatter (FSC) and side scatter (SSC) gating strategy was used to classify cell populations into four quadrants (Q1-Q4) to distinguish cell size and granularity. $CD68.^+$ cells: Macrophages. TUBB3 + cells: Neuron-like differentiated macrophages; (**F**) Immunofluorescence staining to detect the number of NeuN + macrophages after co-culture with NP69 or HK-1 cells (Scale bars = 25 μm). Green represents CD68 + macrophages (1 μg/mL), red represents NeuN + neuron-like cells (1:50), and blue represents DAPI.. The cellular experiments were repeated 3 times, and * indicates a comparison between two groups, * indicates a comparison between two groups, $*p < 0.05$, $**p < 0.01$, $***p < 0.001$

silencing. We identified the sh-TREM2-1 sequence with a high silencing efficacy for further experimental Analysis (Fig. 7I-J). Macrophages with silenced *TREM2* demonstrated lower levels of TUBB3 and NeuN proteins after co-culture, compared to macrophages with unmodified *TREM2* (sh-NC) (Fig. 7K-N).

In conclusion, *TREM2* is believed to be fundamental in initiating the process that converts macrophages into MNT cells.

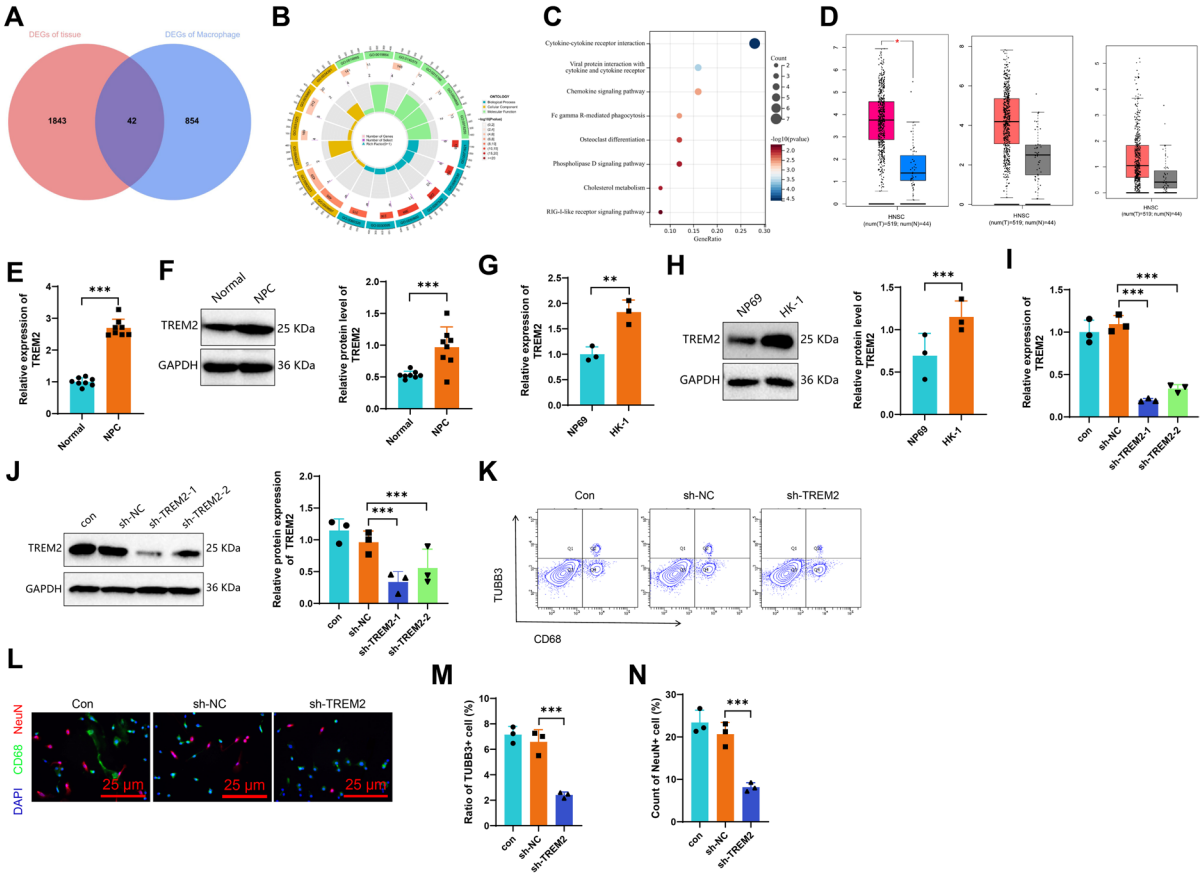

Fig. 7 Investigation of Key Genes Regulating Macrophage Differentiation into MNT in NPC. Note: (**A**) Venn diagram showing the overlapping genes between DEGs in TCGA-NPC and scRNA-seq macrophages; (**B-C**) GO and KEGG enrichment analysis of the intersection genes; (**D**) GEPIA website validation of *TREM2*, *FCGR3 A* and *FCGR3B* expression level in HNSC, where pink represents tumor tissue and blue represents normal tissue; (**E**) RT-qPCR and Western blot experiments were conducted to detect the expression level of *TREM2* mRNA and protein in NPC tumor tissue ($n = 6$); (**F**) Western blot analysis of *TREM2* protein expression in tumor tissues of NPC patients (n = 8); (**G**) RT-qPCR and Western blot experiments were conducted to detect the expression level of *TREM2* mRNA and protein in macrophages co-cultured with NP69 and HK-1 cells; (**H**) Western blot analysis of *TREM2* protein expression in macrophages co-cultured with NP69 and HK-1 cells; (I) RT-qPCR experiment was conducted to detect the silencing efficiency of *TREM2*-specific shRNA; (**J**) Western blot analysis to detect the silencing efficiency of *TREM2*-specific shRNA; (**K-L**) Flow cytometry and immunofluorescence staining experiments were conducted to detect the quantity of TUBB3 +and NeuN +macrophages after silencing *TREM2* and co-culturing with NP69 and HK-1 cells (Scale bars = 50 μm). Green represents CD68 +macrophages (1 μg/mL), red represents $NeuN^+$ neuron-like cells (1:50), and blue represents DAPI. FSC/SSC gating strategy was used to classify cell populations into four quadrants (Q1-Q4) to distinguish cell size and granularity. $CD68^+$ cells: Macrophages. $TUBB3.^+$ cells: Neuron-like differentiated macrophages; (M–N) Statistical results of the quantity of TUBB3 +and NeuN +macrophages after silencing *TREM2* and co-culturing with NHNECs and HK-1 cells using flow cytometry and immunofluorescence staining. The cellular experiments were repeated 3 times, and * indicates a comparison between two groups, $^*p < 0.05$, $^{**}p < 0.01$, $^{***}p < 0.001$

Exploring APOE's Regulatory role on TREM2 in macrophage differentiation

To delve deeper into the genes associated with TREM2 overexpression in macrophages, we developed a network to explore the protein–protein interactions among the proteins encoded by those above 42 overlapping genes (Fig. 8A). Our findings indicate that *TREM2* may interact with *APOE*, *TREM1*, and *CLEC7 A*. Based on the data from the

ChIPBase and GEPIA websites, *TREM2* shows a positive correlation with *APOE*, *TREM1*, and *CLEC7A* in the tumor tissues of HNSC. Additionally, the expression levels of these three genes are upregulated in tumor tissues, as shown in Fig. 8B-C. Related research suggests that *APOE* is linked to cell differentiation and the life activities of macrophages (Ma et al. 2020; You et al. 2020). Thus, it is hypothesized that *APOE* could be linked to the neuronal-like differentiation of microglia activated by *TREM2*.

Furthermore, *APOE* expression was analyzed in both healthy nasopharyngeal epithelial tissues and tumor tissues derived from NPC patients. *APOE* expression was higher in the tumor tissues of NPC patients than in the normal tissues (Fig. 8D). We found a high expression of *APOE* in macrophages when co-cultured with stimulated HK-1 cells (Fig. 8E). To assess *APOE*'s involvement in the transformation of macrophages into MNT cells, we employed a lentiviral transfection technique to introduce a self-designed *APOE*-specific silencing sequence (shRNA) into macrophages. We chose the sh-APOE-2 sequence due to its high silencing efficiency, as depicted in Fig. 8F. Compared to the sh-NC macrophages that were not silenced for *APOE*, the macrophages that were silenced for *APOE* exhibited a drop in the expression levels of TUBB3 and NeuN proteins after co-culture (Fig. 8G-I). The co-culture with *APOE*-silenced macrophages led to a noticeable decline in the levels of both *TREM2* mRNA and protein expression. However, silencing *TREM2* had no impact on the expression of *APOE* (Fig. 8J-K). Moreover, we discovered that the overexpression of *TREM2* in macrophages with silenced *APOE* (sh-APOE + oe-TREM2) could effectively restore the expression levels of TUBB3 and NeuN proteins when co-cultured with HK-1 cells (Fig. 8L-N).

In conclusion, we assert that *APOE* functions as an upstream gene, regulating the expression of *TREM2* in macrophages.

Evaluating the impact of TREM2 silencing in macrophages on pain response and macrophage transformation in an NPC xenograft model

Finally, we further validated the function of *TREM2* in macrophages using an *in vitro* model. Initially, we acquired mouse macrophages with silenced *TREM2* by employing the lentiviral transduction technique (Fig. 9A). We subsequently established an NPC xenograft model in nude mice and depleted macrophages in nude mice using diphtheria toxin. Next, we intravenously injected mouse BMDMs expressing the wildtype control (con), transfected with the vector only (sh-NC), or transfected with the silenced *TREM2* sequence (sh-TREM2) into the nude mice.

Our findings demonstrate that nude mice transplanted with silenced *TREM2* BMDMs display a diminished lick response and withdrawal behavior when touching the site of subcutaneous tumor growth in comparison to nude mice transplanted with normal BMDMs. It indicates a notable decrease in the pain response elicited by BMDMs following *TREM2* silencing (Fig. 9B). Furthermore, both flow cytometry and immunofluorescence analyses demonstrated a notable decrease in the presence of TUBB3 + macrophages within the tumor tissue of nude mice that were transplanted with BMDMs in which *TREM2* was silenced. This finding is illustrated in Fig. 9C-D. According to the findings from *in vitro* experiments, it is hypothesized that the expression of *TREM2* in macrophages of nude mice could attenuate their pain response.

Discussion

This research employs single-cell sequencing technology and TCGA-NPC public data to investigate the cellular heterogeneity of the TME in NPC, with a specific emphasis on macrophage variations. Previous studies have demonstrated that the TME is essential for tumor progression, metastasis, and the efficacy of treatment (Xiao and Yu 2021, Zhang and Zhang 2025). Nevertheless, our comprehension of the intricate interactions among cells and their potential clinical consequences, such as pain, is still limited (Hutlin et al. 2021). This study uncovers a unique subset of microglia relevant to the nervous system, offering us a deeper understanding of the intricate TME.

This study has identified a new subpopulation of neuron-like microglia cells. In contrast to prior research, this study suggests a potential association between the presence of this subgroup in NPC and the experience of chronic pain. This discovery offers a more comprehensive molecular mechanism, elucidating the reasons behind chronic pain experienced by certain patients with NPC. This research offers new perspectives on the function of the APOE-TREM2

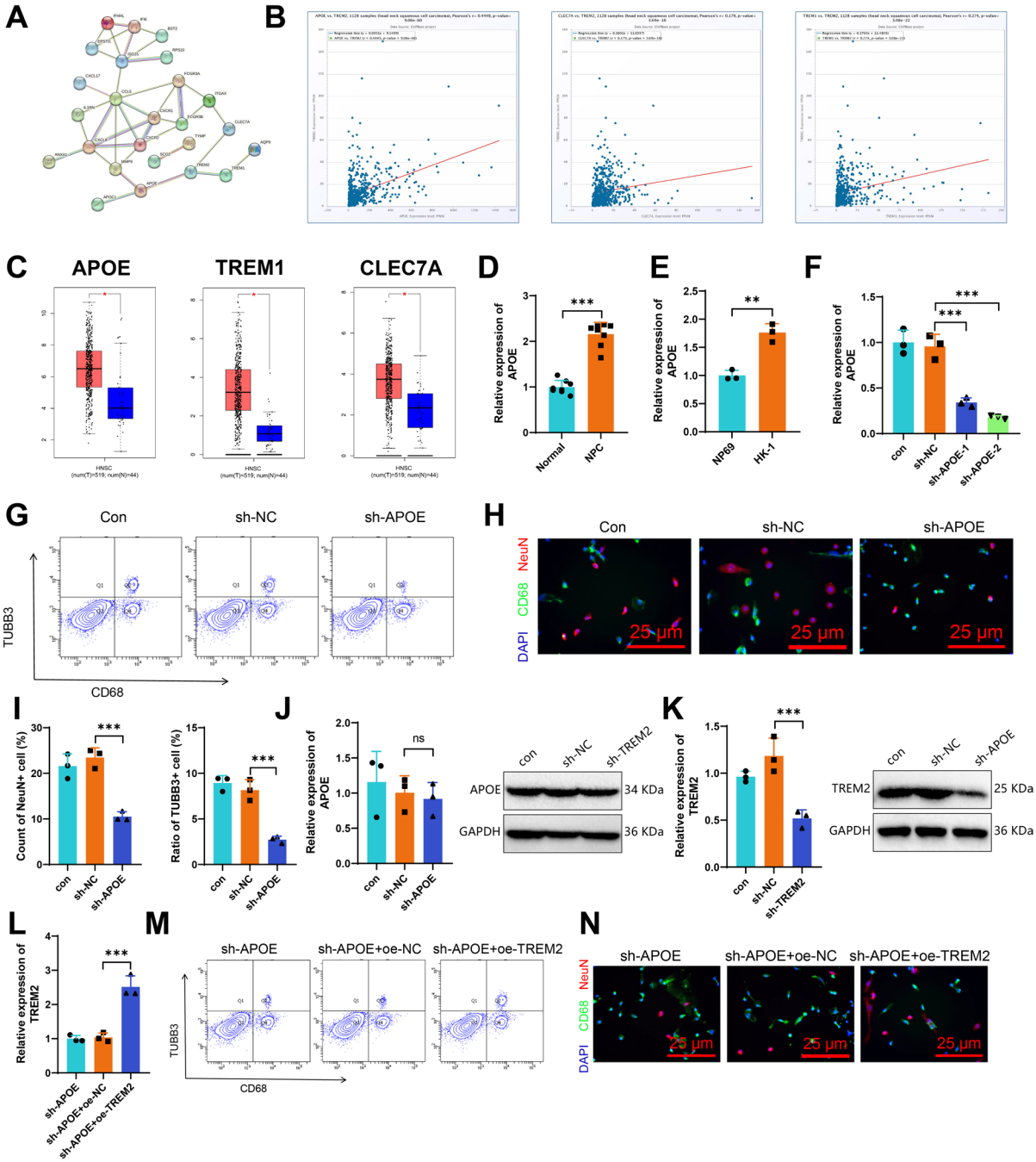

Axis in NPC, specifically in promoting the differentiation of macrophages into neuron-like cells. Research findings indicate that *APOE* and *TREM2* genes were primarily linked to neurodegenerative disorders (Tamura 2021; Huang et al. 2024). Nevertheless, our research indicates that *APOE* and *TREM2* may also have a crucial influence on the initiation and progression of tumors. This novel finding enhances our comprehension of the involvement of *APOE* and *TREM2* in various diseases by offering a fresh biological perspective (Qin et al. 2021).

This study demonstrates that it is possible for tumor cells to induce the transformation of macrophages into neuron-like cells and indicates a

◂**Fig. 8** Investigation of the Mechanism of Macrophage Differentiation into MNT in NPC. Note: (**A**) PPI network of the overlapping 42 genes by String, with a minimum confidence value of 0.7; (**B**) Co-expression relationship of *TREM2* with *APOE*, *TREM1*, and *CLEC7 A* in HNSC tumor tissue determined by ChIPBase website; (**C**) Expression levels of *APOE*, *TREM1*, and *CLEC7 A* in HNSC tumor tissue determined by GEPIA website, where red represents tumor tissue and blue represents normal tissue; (**D**) RT-qPCR experiments were conducted to detect the expression level of *APOE* mRNA in NPC tumor tissue ($n = 8$); (**E**) RT-qPCR experiments were conducted to detect the expression level of *APOE* mRNA in macrophages co-cultured with NP69 and HK-1 cells; (**F**) RT-qPCR experiments were conducted to detect the silencing efficiency of *APOE*-specific shRNA; (**G-H**) Flow cytometry and immunofluorescence staining experiments were conducted to detect the quantity of TUBB3 + and NeuN + macrophages after silencing *APOE* and co-culturing with HK-1 cells (Scale bars = 50 μm). Green represents $CD68^+$ macrophages (1 μg/mL), red represents $NeuN^+$ neuron-like cells (1:50), and blue represents DAPI. FSC/SSC gating strategy was used to classify cell populations into four quadrants (Q1-Q4) to distinguish cell size and granularity. $CD68^+$ cells: Macrophages. $TUBB3^+$ cells: Neuron-like differentiated macrophages; (**I**) Statistical results of the quantity of TUBB3 + and NeuN + macrophages after silencing *APOE* and co-culturing with HK-1 cells using flow cytometry and immunofluorescence staining; (**J**) RT-qPCR and Western blot experiments were conducted to detect the expression level of *APOE* in macrophages after silencing *TREM2* and co-culturing with HK-1 cells; (**K**) RT-qPCR and Western blot experiments were conducted to detect the expression level of *TREM2* in macrophages after silencing *APOE* and co-culturing with HK-1 cells; (**L**) RT-qPCR experiments were conducted to detect the expression level of *TREM2* in macrophages after silencing *APOE* and overexpressing *TREM2* and co-culturing with HK-1 cells; (**M–N**) Flow cytometry and immunofluorescence staining experiments were conducted to detect the quantity of TUBB3 + and NeuN + macrophages after silencing *APOE* and overexpressing *TREM2* in macrophages co-cultured with HK-1 cells(Scale bars = 50 μm). Green represents CD68 + macrophages (1 μg/mL), red represents $NeuN^+$ neuron-like cells (1:50), and blue represents DAPI. FSC/SSC gating strategy was used to classify cell populations into four quadrants (Q1-Q4) to distinguish cell size and granularity. $CD68^+$ cells: Macrophages. $TUBB3.^+$ cells: Neuron-like differentiated macrophages. The cellular experiments were repeated 3 times, and * indicates a comparison between two groups, $^*p < 0.05$, $^{**}p < 0.01$, $^{***}p < 0.001$

potential association between this transformation and chronic pain. It offers a novel approach to managing chronic pain in patients with NPC while also shedding light on the underlying mechanisms responsible for the clinical symptoms observed. Considering the role played by the APOE-TREM2 Axis in the differentiation of macrophages to a neuro-like state, exploring therapeutic strategies that target this axis could provide a new approach for pain relief in patients with NPC. Furthermore, since this transformation is associated with the development of chronic pain, these therapeutic strategies could be deemed for potential employment in the future to prevent or alleviate pain.

In summary, this study presents the following preliminary conclusions: the quantity of macrophages in tumor tissues of patients with NPC correlates with the level of inflammatory response. Additionally, tumor cells stimulate their neuronal-like differentiation by upregulating the APOE-TREM2 Axis in macrophages, thereby facilitating the development of chronic pain in NPC (Fig. 10). Our findings fill a gap in the existing literature regarding cancer pain and neuroimmune interactions. Previous research has mainly focused on the impact of inflammatory mediators on pain, whereas the mechanisms through which tumor-associated macrophages (TAMs) influence neuronal-like differentiation and mediate pain remain unclear (Tang et al. 2022; Domoto et al. 2021). Our study not only elucidates the role of macrophages in NPC-associated chronic pain but also uncovers the molecular mechanism behind this process—neuronal-like differentiation via the APOE-TREM2 Axis. This highlights the novelty and clinical significance of our work. Our findings reveal the role of MNT cells in NPC-related pain, demonstrating the complexity of neuroimmune interactions in cancer pain. This study provides potential mechanistic insights into pain regulation in other cancer types, laying a theoretical foundation for developing novel therapeutic strategies for cancer pain. Our research offers a new perspective on understanding and treating cancer pain, encouraging further exploration of neuroimmune interactions across different cancers, ultimately leading to more precise pain management interventions for cancer patients.

This study utilizes advanced single-cell sequencing technology to unveil a previously unidentified subtype of neuron-like macrophages in the TME. The discovery of this subpopulation of cells may contribute fresh insights into tumor biology and immunology, along with new research directions for future basic and applied studies. Through comprehensive Analysis and research, the pivotal role of this new cell subgroup in the development of chronic pain in NPC has been unraveled. Chronic pain burdens patients, and our current comprehension of its mechanisms remains incomplete. The findings of this study offer fresh perspectives on enhancing the quality of life for patients with NPC. Subsequent research has revealed that the

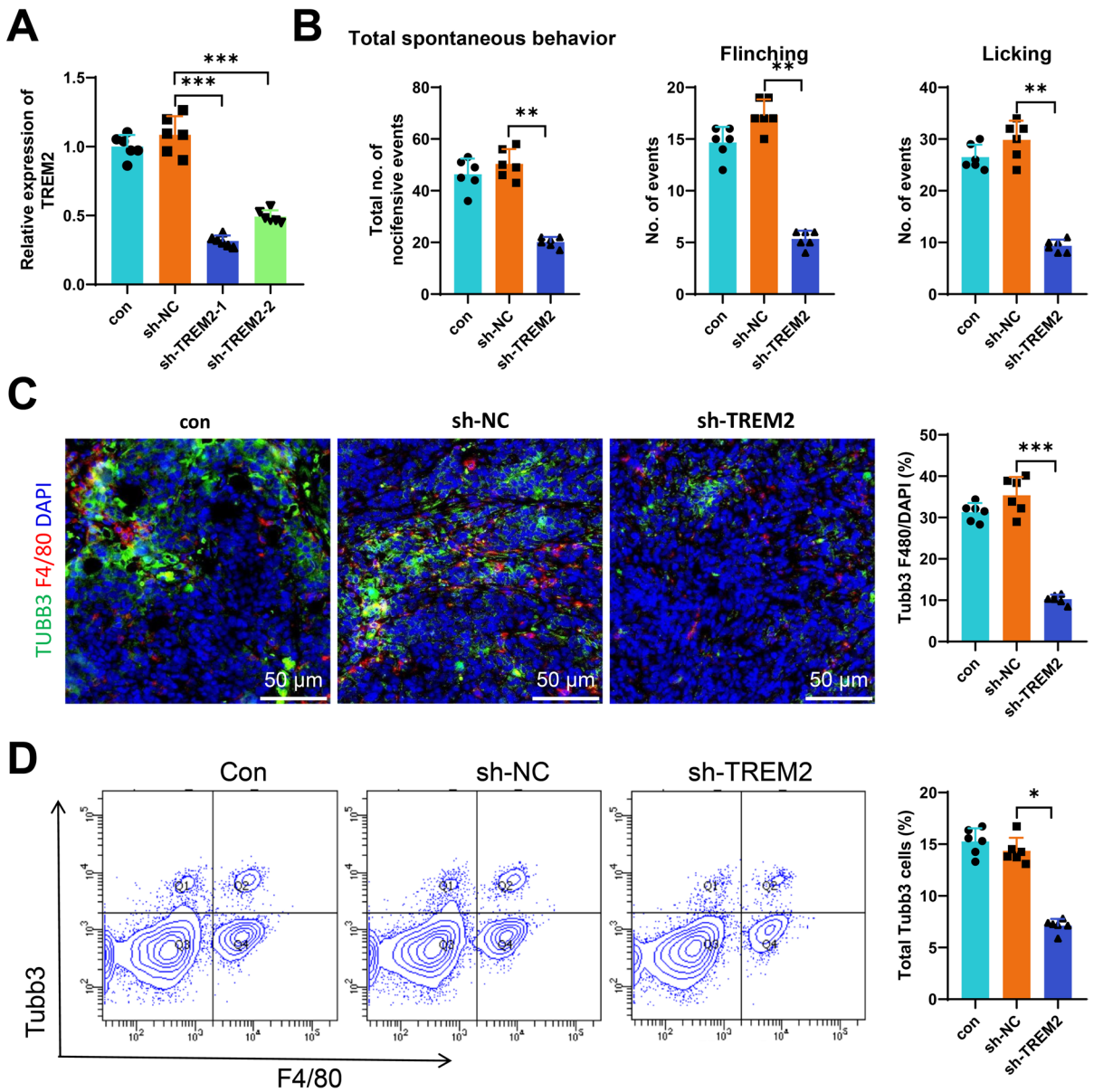

Fig. 9 In vivo Experiment Investigating the Impact of Silencing *TREM2* on Macrophage Differentiation into MNT in NPC. Note: (**A**) RT-qPCR experiment was conducted to detect the silencing efficiency of *TREM2*-specific shRNA; (**B**) Results of pain behavior observation in nude mice on the 20 th day after the start of the Experiment ($n = 6$); (**C**) Immunofluorescence staining experiment was conducted to detect the quantity of TUBB3 + macrophages in different groups of tumor tissue in nude mice ($n = 6$, Scale bars = 50 μm), Green represents TUBB3$^+$ cells (1:50), Red represents F4/80$^+$ macrophages (5 μg/mL), Blue represents DAPI; (**D**) Quantity of TUBB3$^+$ macrophages in different groups of tumor tissue in nude mice ($n = 6$). FSC/SSC gating strategy was used to classify cell populations into four quadrants (Q1-Q4) to distinguish cell size and granularity. TUBB3$^+$ cells: Neuron-like differentiated macrophages. F4/80.$^+$ cells: Macrophages. The cellular experiments were repeated 3 times, and * indicates a comparison between two groups, *$p < 0.05$, **$p < 0.01$, ***$p < 0.001$

TREM2 gene, when regulated by *APOE*, has the potential to induce macrophage transformation into neuron-like cells. This finding provides potential targets for developing novel therapeutic strategies. Treating this mechanism could potentially have an impact on alleviating chronic pain resulting from tumors. Furthermore,

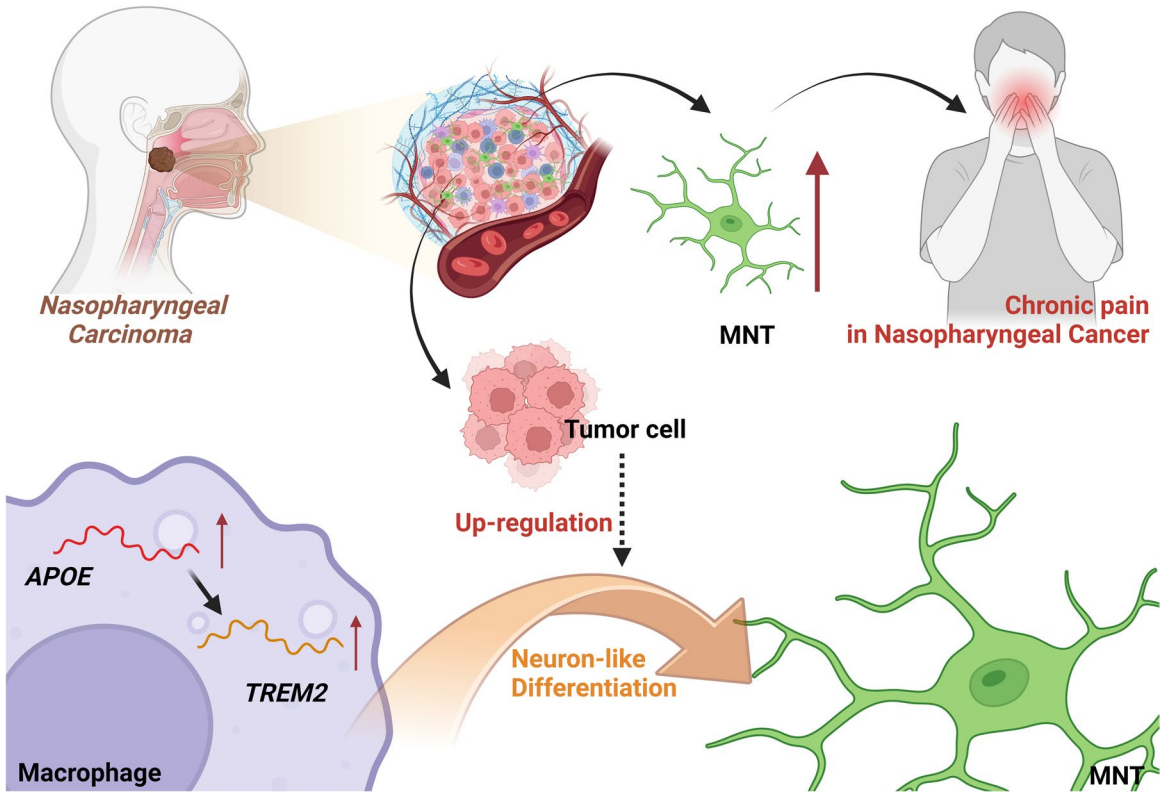

Fig. 10 Molecular mechanisms underlying chronic pain in NPC mediated by tumor cell-induced neuronal-like differentiation through upregulation of the macrophage APOE-TREM2 Axis

our study identifies a novel therapeutic target for cancer pain management by demonstrating that macrophages in NPC mediate chronic pain through neuronal-like differentiation via the APOE-TREM2 Axis. Compared to existing opioid-based or nerve block pain management strategies, interventions targeting the APOE-TREM2 Axis offer greater specificity and may reduce drug resistance and side effects (Chen et al. 2020). For example, developing *TREM2* inhibitors or monoclonal antibodies could effectively block macrophage differentiation and directly alleviate pain. Additionally, such targeted therapies could be combined with immunotherapy to enhance therapeutic efficacy. Future investigations should focus on exploring how these findings can be applied clinically to design tailored pain interventions for NPC patients.

The study did not focus in detail on the impact of systemic inflammation. Systemic inflammation may indirectly influence local macrophage differentiation in NPC through cytokines, chemokines, or metabolic byproducts. The NPC immune microenvironment is highly complex, with multiple immune cell interactions potentially affecting macrophage differentiation. However, due to experimental design and technical limitations, we were unable to fully investigate these interactions. Increase sample size and apply multi-omics analyses to investigate the mechanisms of systemic inflammation. Leverage multicolor flow cytometry and single-cell sequencing to explore how immune cell subsets in the TME are distributed and their functional states, with a focus on their impact on macrophage differentiation.

Despite using the nude mouse subcutaneous transplant tumor model, there remain inherent biological variations between animal models and humans. Thus, the experimental results may not be directly applicable to humans. While this study elucidated the involvement of the macrophage APOE-TREM2 Axis in chronic pain of NPC, the intricate structure of the TME points to the possibility of additional unidentified mechanisms that may be driving chronic pain in NPC. While our study highlights the role of the

APOE-TREM2 Axis in macrophage differentiation and chronic pain in NPC, the TME is highly complex, and other unidentified mechanisms may also contribute to NPC-associated chronic pain. Alternative pathways or compensatory mechanisms should be considered, such as other inflammation-related signaling pathways like *PI3 K-Akt*, which could also influence the TME and pain regulation in NPC (Fang et al. 2022). Although our study establishes a link between the APOE-TREM2 Axis and macrophage differentiation in NPC-associated chronic pain, further investigation into its molecular mechanisms and downstream signaling pathways remains critical. *TREM2*, as an immune receptor, upon activation, regulates various intracellular signaling network, including the *PI3 K-Akt* and *mTOR* pathways, influencing macrophage phagocytosis, proliferation, and metabolic homeostasis (Qiao et al. 2023). Additionally, *TREM2* can regulate inflammatory responses via the *JNK* signaling pathway (Cui et al. 2021). Further research into how the APOE-TREM2 Axis modulates macrophage function through these downstream pathways will provide clearer therapeutic targets for managing NPC-associated chronic pain. Although *TREM2* and *APOE* have been identified as potential therapeutic targets, additional clinical trials are still required to validate their effectiveness in practical clinical applications. And in future research, we plan to combine *in vitro* cell experiments and *in vivo* animal models to further validate whether macrophages can undergo neuronal like differentiation and explore their functions in pain mechanisms. Additional research could be carried out to investigate the biological characteristics of this particular subtype of neuron-like macrophages, as well as their roles in various types of tumors and diseases. To more accurately mimic human diseases, researchers could utilize animal models that closely resemble humans, such as genetically modified mice or humanized mice. Inhibiting the activation of the APOE-TREM2 Axis could effectively block neuronal-like differentiation of macrophages, reduce inflammatory factor release and aberrant neural signaling, thereby alleviating pain and improving the TME. Small-molecule inhibitors could be developed to directly block these signaling pathways, while monoclonal antibodies could precisely target *TREM2* or *APOE*. The potential therapeutic targets identified in this study could undergo drug screening and development and be tested in clinical trials to confirm their application value in treating chronic pain in NPC.

Authors' contributions H.L., L.Z., J.L., and K.Z. contributed equally to this work. H.L. and L.Z. designed and performed the majority of the experiments and data analysis. J.L. conducted the single-cell RNA sequencing analysis and interpreted transcriptomic data. K.Z. was responsible for the in vitro co-culture experiments and molecular assays. W.B. and Y.C. supervised the project, provided critical revisions, and secured funding. All authors contributed to the manuscript writing and approved the final version.

Funding This work was supported by the National Natural Science Fund (No: 81241083), the Science and Technology Department Project of Liaoning Province (Nos: 2021 JH2/10300087), the Science Plan Program of Shenyang City (Nos: 21–172-9–08).

Data availability The datasets generated and/or analyzed during the current study are not publicly available due to privacy and confidentiality agreements with the participants but are available from the corresponding author on reasonable request.

Declarations

Ethics approval and consent to participate This study adheres to the Helsinki Declaration and has obtained informed consent from the patients, as well as approval from the ethics committee of Shengjing Hospital of China Medical University for conducting medical research. All animal experiments conducted in this research institute have received approval from the Animal Ethics Committee of Shengjing Hospital of China Medical University and adhere to local principles for the management and utilization of experimental animals.

Consent for publication Not applicable.

Competing interests The authors declare no competing interests.

References

Caushi JX, Zhang J, Ji Z, Vaghasia A, Zhang B, Hsiue EH-C, et al. Transcriptional programs of neoantigen-specific TIL in anti-PD-1-treated lung cancers. Nature. Springer Science and Business Media LLC; 2021 [cited 2025 Apr 18]. p. 126–32. Available from: https://doi.org/10.1038/s41586-021-03752-4

Chang ET, Ye W, Zeng Y-X, Adami H-O. The Evolving Epidemiology of Nasopharyngeal Carcinoma. Cancer Epidemiol Biomarkers Prev. American Association for Cancer Research (AACR); 2021 [cited 2025 Apr 18]. p. 1035–47. Available from: https://doi.org/10.1158/1055-9965.epi-20-1702

Chen S, Peng J, Sherchan P, Ma Y, Xiang S, Yan F, et al. TREM2 activation attenuates neuroinflammation and neuronal apoptosis via PI3K/Akt pathway after intracerebral hemorrhage in mice. J Neuroinflammation. Springer Science and Business Media LLC; 2020 [cited 2025 Apr 18]. Available from: https://doi.org/10.1186/s12974-020-01853-x

Chen M, Yan X, Hong B, Xiao Y, Qian Y. The Expression and Prognostic Significance of ICOS in NSCLC Integrated Pan-Cancer and Multi-Omics Analyses. Int J Med Sci. Ivyspring International Publisher; 2024 [cited 2025 Apr 18]. p. 795–808. Available from: https://doi.org/10.7150/ijms.93262

Cohen SP, Vase L, Hooten WM. Chronic pain: an update on burden, best practices, and new advances. Lancet. Elsevier BV; 2021 [cited 2025 Apr 18]. p. 2082–97. Available from: https://doi.org/10.1016/s0140-6736(21)00393-7

Cosma N-C, Eren N, Üsekes B, Gerike S, Heuser I, Peters O, et al. Acute and Chronic Macrophage Differentiation Modulates TREM2 in a Personalized Alzheimer's Patient-Derived Assay. Cell Mol Neurobiol. Springer Science and Business Media LLC; 2023 [cited 2025 Apr 18]. p. 3047–60. Available from: https://doi.org/10.1007/s10571-023-01351-7

Cui X, Qiao J, Liu S, Wu M, Gu W. Mechanism of TREM2/DAP12 complex affecting β-amyloid plaque deposition in Alzheimer's disease modeled mice through mediating inflammatory response. Brain Res Bull. Elsevier BV; 2021 [cited 2025 Apr 18]. p. 21–8. Available from: https://doi.org/10.1016/j.brainresbull.2020.10.006

Ding H, Chen S, Pan X, Dai X, Pan G, Li Z, et al. Transferrin receptor 1 ablation in satellite cells impedes skeletal muscle regeneration through activation of ferroptosis. J Cachexia Sarcopenia Muscle. Wiley; 2021 [cited 2025 Apr 18]. p. 746–68. Available from: https://doi.org/10.1002/jcsm.12700

Do TH, Ma F, Andrade PR, Teles R, de Andrade Silva BJ, Hu C, et al. TREM2 macrophages induced by human lipids drive inflammation in acne lesions. Sci Immunol. American Association for the Advancement of Science (AAAS); 2022 [cited 2025 Apr 18]. Available from: https://doi.org/10.1126/sciimmunol.abo2787

Domoto R, Sekiguchi F, Tsubota M, Kawabata A. Macrophage as a Peripheral Pain Regulator. Cells. MDPI AG; 2021 [cited 2025 Apr 18]. p. 1881. Available from: https://doi.org/10.3390/cells10081881

Fang Y, Peng X, Bu H, Jia X, Gao F, Liu C. Chemokine CXCL10 regulates pain behaviors via PI3K-AKT signaling pathway in mice. Neuropeptides. Elsevier BV; 2022 [cited 2025 Apr 18]. p. 102243. Available from: https://doi.org/10.1016/j.npep.2022.102243

Franke M, Bieber M, Kraft P, Weber ANR, Stoll G, Schuhmann MK. The NLRP3 inflammasome drives inflammation in ischemia/reperfusion injury after transient middle cerebral artery occlusion in mice. Brain Behav Immun. Elsevier BV; 2021 [cited 2025 Apr 18]. p. 221–31. Available from: https://doi.org/10.1016/j.bbi.2020.12.009

Hong X, Isern J, Campanario S, Perdiguero E, Ramírez-Pardo I, Segalés J, et al. Mitochondrial dynamics maintain muscle stem cell regenerative competence throughout adult life by regulating metabolism and mitophagy. Cell Stem Cell. Elsevier BV; 2022 [cited 2025 Apr 18]. p. 1298–1314.e10. Available from: https://doi.org/10.1016/j.stem.2022.07.009

Hu F-F, Liu C-J, Liu L-L, Zhang Q, Guo A-Y. Expression profile of immune checkpoint genes and their roles in predicting immunotherapy response. Brief Bioinform. Oxford University Press (OUP); 2020 [cited 2025 Apr 18]. Available from: https://doi.org/10.1093/bib/bbaa176

Huang SH, Jacinto JCK, O'Sullivan B, Su J, Kim J, Ringash J, et al. Clinical presentation and outcome of human papillomavirus-positive nasopharyngeal carcinoma in a North American cohort. Cancer. Wiley; 2022 [cited 2025 Apr 18]. p. 2908–21. Available from: https://doi.org/10.1002/cncr.34266

Huang H, Xiang R, Yan R. Linking APOE4/4 genotype to microglial lipid droplets and neurotoxicity in Alzheimer's disease. Transl Neurodegener. Springer Science and Business Media LLC; 2024 [cited 2025 Apr 18]. Available from: https://doi.org/10.1186/s40035-024-00433-w

Huttlin EL, Bruckner RJ, Navarrete-Perea J, Cannon JR, Baltier K, Gebreab F, et al. Dual proteome-scale networks reveal cell-specific remodeling of the human interactome. Cell. Elsevier BV; 2021 [cited 2025 Apr 18]. p. 3022–3040.e28. Available from: https://doi.org/10.1016/j.cell.2021.04.011

Klein I, Lehmann H. Pathomechanisms of Paclitaxel-Induced Peripheral Neuropathy. Toxics. MDPI AG; 2021 [cited 2025 Apr 18]. p. 229. Available from: https://doi.org/10.3390/toxics9100229

Li K, Zhang S, Sun W, Zhang Y, Yu M, Zhang G, et al. Survival Outcomes Associated With the Size of Opioid Prescriptions in the Management of Chronic Pain Related to Advanced Nasopharyngeal Carcinoma. Ear Nose Throat J. SAGE Publications; 2022 [cited 2025 Apr 18]. p. 014556132211450. Available from: https://doi.org/10.1177/01455613221145093

Liu W, Chen G, Zhang C, Liao X, Xie J, Liang T, et al. Prognostic significance of tumor-infiltrating lymphocytes and macrophages in nasopharyngeal carcinoma: a systematic review and meta-analysis. Eur Arch Otorhinolaryngol. Springer Science and Business Media LLC; 2021 [cited 2025 Apr 18]. p. 25–35. Available from: https://doi.org/10.1007/s00405-021-06879-2

Ma C, Xia R, Yang S, Liu L, Zhang J, Feng K, et al. Formononetin attenuates atherosclerosis via regulating interaction between KLF4 and SRA in apoE-/- mice. Theranostics. Ivyspring International Publisher; 2020 [cited 2025 Apr 18]. p. 1090–106. Available from: https://doi.org/10.7150/thno.38115

Peng Z, Li M, Tan X, Xiang P, Wang H, Luo Y, et al. miR-211–5p alleviates focal cerebral ischemia-reperfusion injury in rats by down-regulating the expression of COX2. Biochem Pharmacol. Elsevier BV; 2020 [cited 2025 Apr 18]. p. 113983. Available from: https://doi.org/10.1016/j.bcp.2020.113983

Qiao X, Wang H, He Y, Song D, Altawil A, Wang Q, et al. Grape Seed Proanthocyanidin Ameliorates LPS-induced Acute Lung Injury By Modulating M2a Macrophage Polarization Via the TREM2/PI3K/Akt Pathway. Inflammation. Springer Science and Business Media LLC; 2023 [cited 2025 Apr 18]. p. 2147–64. Available from: https://doi.org/10.1007/s10753-023-01868-5

Qin Q, Teng Z, Liu C, Li Q, Yin Y, Tang Y. TREM2, microglia, and Alzheimer's disease. Mech Ageing Dev. Elsevier BV; 2021 [cited 2025 Apr 18]. p. 111438. Available from: https://doi.org/10.1016/j.mad.2021.111438

Tamura R. Current Understanding of Neurofibromatosis Type 1, 2, and Schwannomatosis. IJMS. MDPI AG; 2021 [cited 2025 Apr 18]. p. 5850. Available from: https://doi.org/10.3390/ijms22115850

Tang PC-T, Chung JY-F, Liao J, Chan MK-K, Chan AS-W, Cheng G, et al. Single-cell RNA sequencing uncovers a neuron-like macrophage subset associated with cancer pain. Sci Adv. American Association for the Advancement of Science (AAAS); 2022 [cited 2025 Apr 18]. Available from: https://doi.org/10.1126/sciadv.abn5535

Viswanadhapalli S, Dileep KV, Zhang KYJ, Nair HB, Vadlamudi RK. Targeting LIF/LIFR signaling in cancer. Genes Dis. Elsevier BV; 2022 [cited 2025 Apr 18]. p. 973–80. Available from: https://doi.org/10.1016/j.gendis.2021.04.003

Wang L, Gao P, Li C, Liu Q, Yao Z, Li Y, et al. A single-cell atlas of bovine skeletal muscle reveals mechanisms regulating intramuscular adipogenesis and fibrogenesis. J Cachexia Sarcopenia Muscle. Wiley; 2023a [cited 2025 Apr 18]. p. 2152–67. Available from: https://doi.org/10.1002/jcsm.13292

Wang Q, Yu Q, Liu Y. E2F3 renders an immunosuppressive tumor microenvironment in nasopharyngeal carcinoma: Involvements of the transcription activation of PRC1 and BIRC5. Immun Inflam Dis. Wiley; 2023b [cited 2025 Apr 18]. Available from: https://doi.org/10.1002/iid3.987

Wang X, Wu H, Lei F, Liu Z, Shen G, Hu X, et al. Ulinastatin in the treatment of radiotherapy-induced oral mucositis in locoregionally advanced nasopharyngeal carcinoma: a phase 3 randomized clinical trial. Nat Commun. Springer Science and Business Media LLC; 2025 [cited 2025 Apr 18]. Available from: https://doi.org/10.1038/s41467-025-57884-6

Wu K, Liu Y, Shao S, Song W, Chen X, Dong Y, et al. The microglial innate immune receptors TREM-1 and TREM-2 in the anterior cingulate cortex (ACC) drive visceral hypersensitivity and depressive-like behaviors following DSS-induced colitis. Brain Behav Immun. Elsevier BV; 2023 [cited 2025 Apr 18]. p. 96–117. Available from: https://doi.org/10.1016/j.bbi.2023.06.003

Xiao Y, Yu D. Tumor microenvironment as a therapeutic target in cancer. Pharmacol Ther. Elsevier BV; 2021 [cited 2025 Apr 18]. p. 107753. Available from: https://doi.org/10.1016/j.pharmthera.2020.107753

Yan X, Xie Y, Yang F, Hua Y, Zeng T, Sun C, et al. Comprehensive description of the current breast cancer microenvironment advancements via single-cell analysis. J Exp Clin Cancer Res. Springer Science and Business Media LLC; 2021 [cited 2025 Apr 18]. Available from: https://doi.org/10.1186/s13046-021-01949-z

Yang H, Tian W, Zhou B. Sarcopenia and a 5-mRNA risk module as a combined factor to predict prognosis for patients with stomach adenocarcinoma. Genomics. Elsevier BV; 2022 [cited 2025 Apr 18]. p. 361–77. Available from: https://doi.org/10.1016/j.ygeno.2021.12.011

Yassen SS, Al-Badri SG, Aldarawsha AN, Elazab MS, Alawad A, Hameedi AD, et al. Nasopharyngeal carcinoma with unusual metastatic spread to the spine and meninges: a case report with literature review. J Surg Case Rep. Oxford University Press (OUP); 2024 [cited 2025 Apr 18]. Available from: https://doi.org/10.1093/jscr/rjaf022

Yim A, Smith C, Brown AM. Osteopontin/secreted phosphoprotein-1 harnesses glial-, immune-, and neuronal cell ligand-receptor interactions to sense and regulate acute and chronic neuroinflammation. Immunol Rev. Wiley; 2022 [cited 2025 Apr 18]. p. 224–33. Available from: https://doi.org/10.1111/imr.13081

You Y, Bao W-L, Zhang S-L, Li H-D, Li H, Dang W-Z, et al. Sorting Nexin 10 Mediates Metabolic Reprogramming of Macrophages in Atherosclerosis Through the Lyn-Dependent TFEB Signaling Pathway. Circ Res. Ovid Technologies (Wolters Kluwer Health); 2020 [cited 2025 Apr 18]. p. 534–49. Available from: https://doi.org/10.1161/circresaha.119.315516

Yousuf MS, Shiers SI, Sahn JJ, Price TJ. Pharmacological Manipulation of Translation as a Therapeutic Target for Chronic Pain. Pharmacol Rev. Elsevier BV; 2021 [cited 2025 Apr 18]. p. 59–88. Available from: https://doi.org/10.1124/pharmrev.120.000030

Zhang Y, Gong G, Qiu Q, Han Y, Lu H, Yin Y. Radiomics for Diagnosis and Radiotherapy of Nasopharyngeal Carcinoma. Front Oncol. Frontiers Media SA; 2022 [cited 2025 Apr 18]. Available from: https://doi.org/10.3389/fonc.2021.767134

Zhang Y, Sang R, Bao J, Jiang Z, Qian D, Zhou Y, et al. Schwann cell-derived CXCL2 contributes to cancer pain by modulating macrophage infiltration in a mouse breast cancer model. Brain Behav Immun. Elsevier BV; 2023 [cited 2025 Apr 18]. p. 308–20. Available from: https://doi.org/10.1016/j.bbi.2023.02.004

Zhang M, Zhang B. Extracellular matrix stiffness: mechanisms in tumor progression and therapeutic potential in cancer. Exp Hematol Oncol. Springer Science and Business Media LLC; 2025 [cited 2025 Apr 18]. Available from: https://doi.org/10.1186/s40164-025-00647-2

Zhu L, Duan W, Peng L, Shan X, Liu Y, Huang Z, et al. A novel proteomic prognostic signature characterizes the immune landscape and predicts nasopharyngeal carcinoma prognosis. Heliyon. Elsevier BV; 2024 [cited 2025 Apr 18]. p. e37897. Available from: https://doi.org/10.1016/j.heliyon.2024.e37897